Cold Regions Science and Technology 236 (2025) 104497

Contents lists available at ScienceDirect

Cold Regions Science and Technology

journal homepage: www.elsevier.com/locate/coldregions

State of the art of mechanical behaviors of frozen soils through experimental investigation

Kai-Qi Li [a], Zhen-Yu Yin [a,*], Zhao-Hui Yang [b], Yong Liu [c]

[a] Department of Civil and Environmental Engineering, The Hong Kong Polytechnic University, Hung Hom, Kowloon, Hong Kong, China
[b] Civil Engineering Department, University of Alaska Anchorage, Anchorage, AK 99508, USA
[c] State Key Laboratory of Water Resources Engineering and Management, Wuhan University, Wuhan, Hubei, China

ARTICLE INFO

Keywords:
Frozen soil
Mechanical behavior
Static and dynamic loading
Stress-strain relationship
Microstructural analysis

ABSTRACT

Frozen soils exhibit unique mechanical behavior due to the coexistence of ice and unfrozen water, making experimental studies essential for engineering applications in cold regions. This review comprehensively examines laboratory investigations on frozen soils under static and dynamic loadings, including uniaxial and triaxial compression, creep, direct shear, and freeze-thaw (F-T) cycle tests. Key findings on stress-strain characteristics, failure mechanisms, and the effects of temperature and time are synthesized. Advancements in microstructural analysis techniques, such as computed tomography (CT), scanning electron microscopy (SEM), nuclear magnetic resonance (NMR), and mercury intrusion porosimetry (MIP), are also summarized to elucidate the internal structural evolution of frozen soils. While significant progress has been made, further efforts are needed to better replicate complex environmental and loading conditions and to fully understand the interactions between multiple influencing factors. Future research should focus on developing novel experimental techniques, establishing standardized testing protocols, and creating a comprehensive database to enhance data accessibility and advance frozen soil research. This review provides critical insights into frozen soil mechanics and supports validating constitutive models and numerical simulations, aiding infrastructure design and construction in cold regions.

1. Introduction

In recent decades, frozen ground engineering has experienced significant advancements driven by the increasing demand for infrastructure development in cold regions. The mechanical behaviors of frozen soils are closely associated with several engineering problems, such as slope instability and subgrade settlement (Li and Yin, 2024; Li et al., 2024a, 2024b). Moreover, frozen soils play significant roles in engineering construction in permafrost regions and the implementation of artificial ground freezing (AGF) methods in mining and urban constructions, including tunnels, shafts, and deep excavations under challenging ground conditions (Liu et al., 2022a; Li et al., 2023b, 2023c; Li et al., 2024a, 2024b). The mechanical behaviors of frozen soils also serve as the basis for evaluating the stability and ensuring the safety of the corresponding structures or engineering projects. Therefore, it is necessary to capture and determine frozen soils' mechanical behaviors accurately.

As a typical composite material, frozen soil consists of four components: soil mineral particles, liquid water, gaseous inclusions, and ice crystals (Li et al., 2020a; Li et al., 2023a). The mechanical behaviors of frozen soils are more complicated than those of unfrozen soils due to frozen soil's complex configurations (or cryostructure) and their higher sensitivity to temperature (Bray, 2012; Lai et al., 2013; Li et al., 2022; Li et al., 2025), particularly near the phase transformation temperature (e.g., 0 °C). The temperature effect stems from two aspects. The first is that the ice properties are significantly dependent on the temperature. Many scholars (e.g., Smith and Schulson, 1994; Gagnon and Gammon, 1995; Fish and Zaretsky, 1997; Xu et al., 2011a, 2011b) have explored the characteristics of ice, but there is no consensus on the shear strength of ice. Generally, it is acknowledged that the shear strength of ice exhibits an inverse relationship with decreasing temperature. Additionally, the shear strength of ice shows a nonlinear correlation with confining pressure and is positively influenced by the strain rate (Rist and Murrell, 1994; Jones, 1982). Besides, the ice content is also strongly dependent on the temperature, especially for fine-grained soils due to their higher water retention capacity. The second is the bonding strength of the

* Corresponding author.
E-mail addresses: kqcee.li@polyu.edu.hk (K.-Q. Li), zhenyu.yin@polyu.edu.hk (Z.-Y. Yin), zyang2@alaska.edu (Z.-H. Yang), liuy203@whu.edu.cn (Y. Liu).

https://doi.org/10.1016/j.coldregions.2025.104497
Received 9 September 2024; Received in revised form 25 February 2025; Accepted 22 March 2025
Available online 24 March 2025

interface between soil particles and ice, which is also highly related to temperature. In most cases, the strength can improve with decreasing temperature, leading to an enhanced capacity to resist external deformation. Besides, the impact of temperature variation on mechanical behaviors is generally different under various stress levels, indicating that temperature's effect is more complex. In general, the mechanical properties of frozen soils are affected by soil type, ice content, unfrozen water, dry density, mineralogy composition, temperature, confining pressure, freeze-thaw process, loading paths, and so on (e.g., Johnson et al., 1979; Qi and Ma, 2007; Zhu et al., 2016; Yao et al., 2017).

A large number of mechanical tests under static and dynamic loadings have been conducted. Previous experimental tests have discussed the influences of external environmental factors and soil properties, but few have considered all the critical influencing factors and their joint effects. Given that numerous studies on static and dynamic tests of frozen soils, herein, the typical investigations in recent two decades have been checked (see Fig. 1, topics are "frozen soil", "mechanical behaviors", and "test" in the Web of Science, contributions from pre-2003 research and conference papers are not fully represented here). It can be noted that the experimental studies on frozen soils are growing exponentially.

To further illustrate the primary research themes in frozen soil mechanical behaviors studies, Fig. 2 presents a co-occurrence network of keywords from existing literature. The visualization highlights "mechanical properties", "freeze-thaw cycles", "soil", and "strength" as central themes, indicating their dominant role in frozen soil research. These topics are strongly interconnected with other key aspects, such as "microstructure", "compressive strength", "constitutive model", "temperature" and "strain". Secondary focuses, including "permafrost", "durability", and "stabilization" reveal the practical and diverse applications of frozen soil mechanics in engineering and environmental studies.

This study provides a comprehensive review of experimental investigations on frozen soils under static and dynamic loads. Section 2 systematically examines various types of static tests, while Section 3 summarizes existing studies on frozen soils subjected to dynamic loading. Section 4 reviews recent advancements in microstructural analysis of frozen soils. Section 5 discusses key advancements in experimental techniques and microstructural observations and explores potential extensions to frozen soil analogs. Finally, the concluding section highlights key findings and discusses future research directions in experimental testing of frozen soils. This study enhances the understanding of the complex mechanical behavior of frozen soils and serves as a valuable reference for constitutive modeling, engineering design, and maintenance in cold regions.

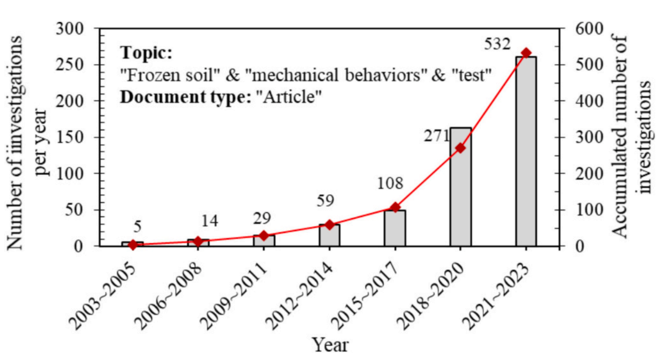

Fig. 1. Number of investigations of experimental tests on frozen soils in recent two decades (from 2003 to 2023), based on records available in the Web of Science database.

2. Mechanical behaviors under static loading

2.1. Experimental methodology

To date, numerous experimental tests under static loadings have been widely conducted to examine the effects of various factors (e.g., temperature, confining pressure, strain rate, stress path, and stress level) on the mechanical properties of frozen soils, which play a significant role in understanding the response of frozen soils under static loadings and provide essential data for the development of constitutive models and engineering design (He et al., 2023; Yu et al., 2024; Xu et al., 2025; Zhang et al., 2025).

In general, laboratory tests conducted on undisturbed frozen soil samples tend to yield results that are closer to real-world conditions. However, utilizing undisturbed frozen soil in laboratory testing presents various challenges, including the complexities associated with sampling and transporting soil from the field and the inherent irregularity within undisturbed frozen soil samples, which can lead to inconsistent test results. Consequently, remolded frozen soil specimens are prepared with standardized structures, which enables consistent test results and facilitates the comprehensive analysis of the influence of various factors on the mechanical properties of frozen soils. Accordingly, the majority of the experiments documented in the literature have been conducted on remolded samples in addition to some studies (i.e., Cui et al., 2014; Yang et al., 2015; Wang et al., 2019c; Li et al., 2020b) that collected in situ undisturbed soils in an unfrozen state and then subjected them to freezing before testing. Only one study (Shastri et al., 2021) reported in-situ testing of natural frozen soils directly in their frozen state in Alaska. To simulate the real-world conditions of frozen soils, diverse parameters, such as temperature, moisture content, and soil composition, are taken into account. Subsequently, the frozen soil samples are subjected to static loadings employing specialized testing equipment.

According to test types, existing experiments are divided into four categories, i.e., triaxial compression tests, uniaxial compression tests, creep tests and other tests. Tables 1–4 list the experimental tests on frozen soils under static loadings that have significantly contributed to the active research on the mechanical behavior of frozen soils in the last few decades. Besides, detailed information on test conditions and frozen soil samples is summarized in Tables 1–4. It can be noted that various tests have investigated frozen soil's mechanical characteristics under different testing conditions, including temperature, strain rate, confining pressure, and so on.

Table 1 summarizes key studies on triaxial compression tests of frozen soils, focusing on those that provide significant contributions to understanding the mechanical behaviors of frozen soils under varying conditions. The studies were selected based on their relevance, methodological rigor, and representation of diverse factors such as temperature, confining pressure, strain rate, and freeze-thaw cycles. A clear trend emerges from the table, highlighting a progressive shift in research focus. Early studies primarily investigated the fundamental effect of temperature (e.g., Chamberlain et al., 1972; Sayles, 1974), laying the groundwork for understanding frozen soil mechanics. More recent studies (e.g., Lai et al., 2014; Zhou et al., 2016) have integrated advanced testing systems, such as MTS-810, to explore the combined effects of multiple factors, including stress paths, freeze-thaw cycles, and material composition (e.g., salt and coarse-grain content). These advancements reflect an increasing emphasis on simulating complex real-world engineering conditions.

Additionally, there has been a growing trend in the measurement and analysis of volumetric strain during triaxial tests. While earlier studies often neglected volumetric strain, recent research (e.g., Xu et al., 2016; Liu et al., 2019) has increasingly incorporated advanced volume-measuring devices to capture these changes. This shift highlights the need to account for the coupling between stress-induced deformation and ice phase transitions, particularly under varying confining pressures and temperatures. The ability to measure volumetric strain has provided

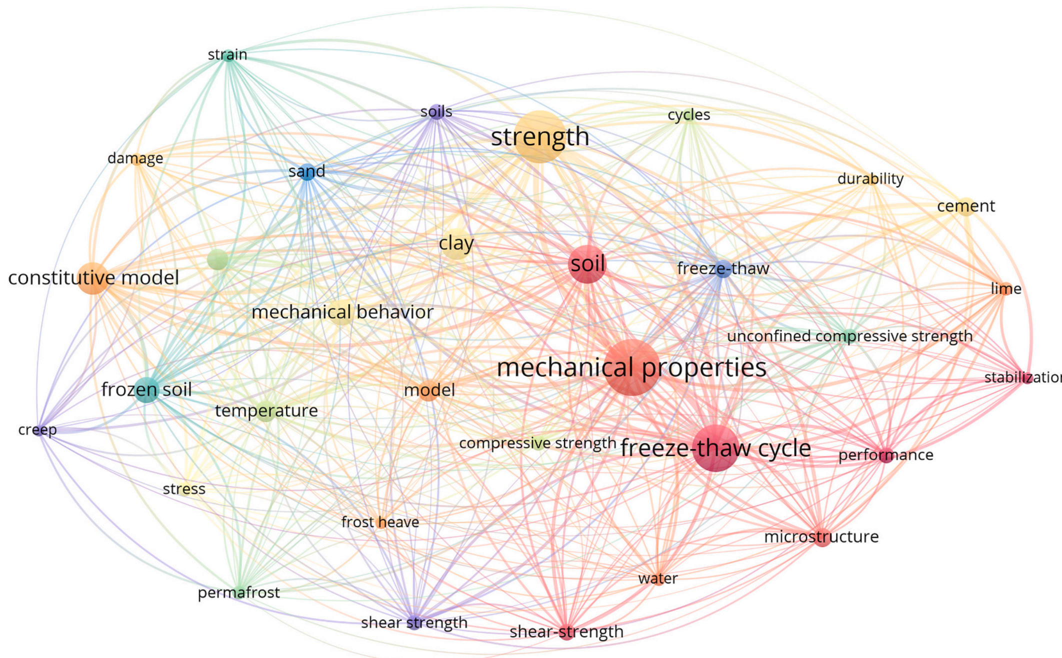

Fig. 2. Co-occurrence network of keywords from existing studies on mechanical behaviors of frozen soils.

deeper insights into mechanisms such as dilation, compression, and ice-water interactions during shearing. Yao et al. (2013) developed a versatile triaxial apparatus for frozen soils, featuring precision control of temperature and K_0-state, along with the capability to accurately measure volumetric changes. These advancements demonstrate the field's progression from basic parameter studies to more comprehensive investigations that integrate both stress-strain and volumetric responses, enabling a better understanding of frozen soil behavior in practical engineering scenarios.

It is concluded that existing triaxial compression tests are limited in their ability to simulate true triaxial conditions, as they cannot independently control the intermediate principal stress. Recent advancements, such as the novel true triaxial testing system developed by Huang et al. (2022), offer a promising approach to investigate the strength and deformation properties of frozen soils under general stress states. Additionally, the stochastic effects of ice lenses, such as their spatial distribution, orientation, and interconnectivity, play a significant role in the mechanical behaviors of frozen soils but remain underexplored.

To better understand the mechanical behavior of frozen soil under complex loading conditions, researchers have employed static cyclic loading-unloading (SCLU) tests and stress path experiments. These methods provide deeper insights beyond conventional triaxial tests, capturing the effects of elastoplastic coupling, damage evolution, energy dissipation, and loading history. Early studies by Xu et al. (2011a, 2011b), Xu et al., 2014) utilized the MTS-810 triaxial apparatus to investigate the mechanical behavior of frozen soil under different loading paths, including uniaxial and triaxial cyclic loading-unloading tests. Xu et al. (2015) conducted a series of SCLU tests on frozen loess to analyze energy dissipation and damage characteristics, offering a quantitative approach to defining damage variables. Shen et al. (2022) explored the effect of stress paths on frozen subgrade soil through six different linear stress paths, highlighting the influence of stress history on deformation and strength evolution. Wang et al. (2023) extended this research by designing 32 distinct stress paths for frozen silty clay, providing a comprehensive understanding of frozen soil mechanical behavior under complex conditions.

Fig. 3(a) illustrates the number of studies reviewed in this study that focus on certain influencing factors, which shows that most previous triaxial tests have comprehensively explored the impact of temperature and confining pressure on mechanical behaviors. Some scholars have also conducted uniaxial compression (UC) tests on frozen soils (see Table 2). The UC test is generally capable of characterizing the mechanical properties of frozen soils, especially shallow frozen soils. Fig. 3 (b) depicts the influencing factors considered in these uniaxial tests, which demonstrated that most studies addressed the impacts of temperature on the mechanical behaviors of frozen soils in uniaxial compression tests. In addition to the effect of temperature, strain rate, freeze-thaw (F-T) cycles, and some soil parameters were also incorporated in these previous uniaxial studies.

As summarized in Table 3, many scholars have conducted creep tests of frozen soils to explore the long-term deformation characteristics under various complex conditions, including temperature, confining pressure, thermal gradient, stress path and history, coarse grain content, and heterogeneous structures. Additionally, other experimental tests are conducted to assess the mechanical properties of frozen soils (see Table 4), such as tension tests, direct shear tests, directional shear tests, small-stain loading tests, and stress relaxation tests. The outcomes derived from these tests significantly contribute to characterizing the stress-strain behavior and crucial mechanical properties of frozen soils. Experimental tests conducted under static loading conditions offer essential insights into frozen soils' mechanical properties and behaviors. These static tests play a crucial role in formulating accurate constitutive models that capture the mechanical response of frozen soils and provide valuable guidance for designing and constructing infrastructure projects in cold regions where frozen soils are prevalent.

2.2. *Mechanical behaviors*

The mechanical behavior of frozen soils under static loading is a critical area of research due to its importance in understanding the performance of infrastructure in cold regions. Frozen soils exhibit unique mechanical properties influenced by the coexistence of soil particles, ice, and unfrozen water. These properties are heavily affected by internal factors (e.g., soil type, ice content, moisture content, and salinity) and external environmental conditions (e.g., temperature, strain rate, confining pressure, and freeze-thaw cycles). Table 5 summarizes frozen soils' typical static mechanical behaviors under different external loads and internal factors.

Table 1
Summary of triaxial compression tests on frozen soils.

No.	Refs.	Test conditions							Frozen soil samples									
		Factors	ε_v	Devices	T (°C)	σ_3 (MPa)	$\dot{\varepsilon}$ (/s)	FTC	Types	Locations	Size (mm)	G_s	ω (%)	ρ_{dry} (g/cm^3)	LL (%)	PL (%)	f_s (%)	f_c (%)
1	Chamberlain et al., 1972	σ_3	Y	TA	−10	3.45–275.79	0.001	–	Ottawa sand, silt	US (New Hampshire)	ϕ35.56 × 88.9	2.63, 2.84	19.9–22, 17.9–19.5	1.62–1.67, 1.77–1.81	-, 16	–	–	–
2	Sayles, 1974	σ_3, $\dot{\varepsilon}$	N	TA	−3.85	0.34–8.2	3.33×10^{-5}–1.67×10^{-2}	–	Ottawa sand	–	ϕ70 × 152.5	2.65	18.8–25.1	1.67	–		–	–
3	Parameswaran and Jones, 1981	σ_3	N	TA (MTS)	−10	0.1–75	7.7×10^{-5}	–	Ottawa sand	US (Illinois)	ϕ50.8 × 108	–	20	–	–	–	–	–
4	Wang et al., 2004	T, σ_3	N	TA (MTS-810)	−2, −5, −7, −10	1–5	–	–	Loess	China (Lanzhou)	ϕ61.8 × 125	–	16.5	1.78	24.6	17.7	–	–
5	Wang et al., 2005	Soil type, loading way, T, σ_3	N	TA (MTS-810)	−2, −5, −7, −10	1–5	–	–	Sand, loess	China (Lanzhou)	ϕ61.8 × 125	–	10.5, 16.5	2, 1.78	-, 24.6	-, 17.7	–	–
6	Qi and Ma, 2007	σ_3, T	N	TA (MTS)	−2, −3.5, −7	2–20	1.1×10^{-3}	–	Fine sand	China (Lanzhou)	ϕ61.8 × 150	–	24.2	15.6	–	–	–	–
7	Zhang et al., 2007	Soil type, T, σ_3	Y	TA (MTS-810)	−4, −6	0.3–18	1.67×10^{-4}	–	Sandy clay, silty clay	China (Qinghai–Tibet Railway)	ϕ61.8 × 125	–	–	–	14.9	24.5	–	–
8	Lai et al., 2008	Soil type, T	N	TA (MTS)	−0.5, −1, −2	–	1.67×10^{-4}	–	Warm clay, warm ice-rich clay	China (Qinghai–Tibet Railway)	ϕ61.8 × 125	–	–	–	–	–	–	–
9	Lai et al., 2009	σ_3	N	TA (MTS)	−6	1–18	1.67×10^{-4}	–	Sandy clay	China (Qinghai–Tibet Railway)	ϕ61.8 × 125	–	12.7	1.97	–	–	–	–
10	Lai et al., 2010b	T, σ_3	Y	TA (MTS-810)	−2, −4, −6	1–14	1.67×10^{-4}	–	Silt	China (Qinghai–Tibet Railway)	ϕ61.8 × 125	–	12.8	–	23.2	15	–	–
11	Yang et al., 2010b	σ_3, ω	Y	TA (MTS-810)	−6	0.5–14	1.67×10^{-4}	–	Sand	–	ϕ61.8 × 125	–	10, 15, 20	1.95, 1.81, 1.68	–	–	–	–
12	Yang et al., 2010c	σ_3	Y	TA (MTS-810)	−6	4–14	1.67×10^{-4}	–	Silt	–	ϕ61.8 × 125	–	12.8	1.81	–	–	–	–
13	Yang et al., 2010d	σ_3	N	TA (MTS-810)	−4	0.5–14	1.67×10^{-4}	–	Sand	–	ϕ61.8 × 125	–	15	1.85	–	–	–	–
14	Cui et al., 2014	σ_3	N	–	−20	0.1–0.35		–	Silty clay	–	ϕ39.1× 80	–	–	–	–	–	–	–
15	Xu, 2014	T, σ_3	Y	–	−1, −2, −5, −10; −4, −6	1; 0.3–1	1.67×10^{-4}	–	Sand	–	ϕ61.8 × 125	–	–	1.82	–	–	–	–
16	Lai et al., 2014	Stress path, σ_3	Y	TA (MTS-810)	−6	0.5–17,-, (2–5)	1.67×10^{-4}	–	Loess	China (Lanzhou)	ϕ61.8 × 125	2.69	17	2.01	27	15.4	–	–
17	Yang et al., 2015	Stress level, σ_3	Y	TA (MTS-810)	−8	0.5–3	1.67×10^{-4}	–	Frozen silt	–	ϕ61.8 × 125	–	–	–	–	–	–	–
18	Lai et al., 2016	f_s, σ_3	Y	TA (MTS-810)	−6	0–16	1.67×10^{-4}	–	Sandy	–	ϕ61.8 × 125	–	13	1.89	23.2	15	0.0 %, 0.5 %, 1.5 %, 2.5 % (Na_2SO_4)	–
19	Xu et al., 2016	T, σ_3	Y	TA	(−1, −2, −5, −10), −4	1, (0.3, 0.6, 0.8, 1)	1.67×10^{-4}	–	Sand, frozen silty sand	China (Xiamen)	ϕ61.8 × 125	–	–	1.82	–	–	–	–
20	Zhou et al., 2016	T, σ_3	Y	TA	−3, −6, −9	1–15	4×10^{-4}	–	Frozen loess	China (Lanzhou)	ϕ62 × 125		16.5	1.78	–	–	–	–

(*continued on next page*)

Table 1 (*continued*)

No.	Refs.	Test conditions							Frozen soil samples									
		Factors	ε_v	Devices	T (°C)	σ_3 (MPa)	$\dot{\varepsilon}$ (/s)	FTC	Types	Locations	Size (mm)	G_S	ω (%)	ρ_{dry} (g/cm^3)	LL (%)	PL (%)	f_s (%)	f_c (%)
21	Liao et al., 2017	f_s, σ_3	N	TA (MTS-810)	−6	2–16	–	–	Frozen saline soils	China (Qinghai–Tibet Railway)	ϕ61.8 × 125	–	–	–	–	–	0.0 %, 0.5 %, 1.5 %, 2.5 % (Na_2SO_4)	–
22	Wang et al., 2017	T, $\dot{\varepsilon}$		TA	−2, −5, −10	–	1.67×10^{-5}, 1.67×10^{-6}, 1.67×10^{-7}	–	Kasaoka clay	Japan	ϕ30 × 60	2.65	36.63–51.01	1.709–1.848	62	28	–	–
23	Xu et al., 2017a	T, f_s, σ_3	N	TA (MTS-810)	−3, −5, −7	0.3–6	–	–	Silty sand	China (Ningxia Hui Autonomous Region)	ϕ61.8 × 125	–	–	1.87	–	–	1 % (NaCl)	–
24	Esmaeili-Falak et al., 2018	T, σ_3, $\dot{\varepsilon}$, σ_3	N	–	−1 ~ −11	0, 0.05, 0.1, 0.2, 0.4, 0.8	1.67×10^{-5}, 3.33×10^{-5}, 8.33×10^{-5}, 1.67×10^{-4}, 3.33×10^{-4}	–	Sand, clay	Iran	ϕ50 × 100	2.635, 2.7	–	1.98, 2.11	49	24	–	–
25	Nassr et al., 2018	T, σ_3, $\dot{\varepsilon}$	N	–	−0.5 ~ −11	0–0.8	1.67×10^{-5}, 3.3×10^{-4}	–	Sand	–	ϕ50 × 100	–	–	–	–	–	–	–
26	Tang et al., 2018	FTC	N	–	−10	0.1, 0.2, 0.3	1.67×10^{-3}	Cycles = 1, 3, 5, 9; T_t = 10 °C	Expensive soil	China (Jilin Province)	ϕ39.1 × 80	–	27	1.65	53	38	–	–
27	Yao et al., 2018	T	N	Multifunction environmental testing apparatus	Increase from −10	–	–	–	Sand	–	ϕ61.8 × 125	–	16.3–16.8	1.75–1.77	–	–	–	–
28	Zhou et al., 2018	FTC, σ_3, T	N	TA (MTS-810)	−6, −12	–	–	Cycles = 0, 3, 6, 9, 12; T_t = 15 °C	Loess	China (Lanzhou)	ϕ62 × 125	–	–	–	17.4	25.7	–	–
29	Chang et al., 2019	f_s, σ_3	Y	–	−6	0–16	1.67×10^{-4}	–	Sandy	–	ϕ61.8 × 125	–	–	1.85	–	–	0, 0.5, 1.5, 2.5, 3.5 (Na_2SO_4)	–
30	Liu et al., 2019	f_c, T, σ_3	Y	–	−6, −10, −15	0.3–15	1.48×10^{-4}	–	Silty clay with coarse sand	China (Lanzhou)	ϕ61.8 × 125	2.66	–	–	–	–	–	20, 40, 60, 80, 100
31	Nishimura et al., 2019	T	N	TA	−2, −5, −10	0.1, 0.2, 0.4	1.67×10^{-5}, 1.6×10^{-6}, 1.33×10^{-7}		Clay	–	ϕ30 × 60		0.596	0.225	–	–	–	–
31	Yao et al., 2019	$\dot{\varepsilon}$, σ_3	N	–	−5	0.5–10	1.67×10^{-4}, 1.67×10^{-5}, 1.6×10^{-6}, 1.33×10^{-7}	–	Sand	–	ϕ61.8 × 125	–	16.2–16.8	1.74–1.78	–	–	–	–
32	Zhang et al., 2019a, 2019b, 2019c	σ_3	Y	TA (MTS-810)	−5	0.3–2	1.48×10^{-4}	–	Silt soils	China (Lanzhou)	ϕ61.8 × 125	–	15	1.9	27.58	13.7	–	–
33	Zhang et al., 2019b	σ_3	N	TA (MTS-810)	−6	0.3–1.8	1.67×10^{-4}	–	Sand	–	ϕ61.8 × 125	–	–	1.78	–	–	–	–
34	Li et al., 2020c	T, σ_3	N	Self-developed W3Z-200 testing system	−5, −10, −15	3–7	–	–	Clay	China (Huainan)	ϕ61.8 × 125	–	–	–	–	–	–	–

(*continued on next page*)

Table 1 (*continued*)

No.	Refs.	Test conditions							Frozen soil samples									
		Factors	ε_v	Devices	T (°C)	σ_3 (MPa)	$\dot{\varepsilon}$ (/s)	FTC	Types	Locations	Size (mm)	G_S	ω (%)	ρ_{dry} (g/cm^3)	LL (%)	PL (%)	f_s (%)	f_c (%)
35	Zhang et al., 2020a	ω, T, σ_3	N	TA	−2, −4	0.5–4	1.67×10^{-4}	–	Silty clay	China (Qinghai–Tibet region)	ϕ61.8 × 125	–	15, 30, 50	–	31.87	17.44	–	–
36	Nishimura et al., 2021	FTC, T	N	TA	−5, −10, −20	–	–	Cycles =5, T_t = 25 °C	Kasaoka clay, silty clay	–	ϕ30 × 60	–	–	2.65, 2.59	62, 46	28, 32	–	–
37	Pham et al., 2021	T, σ_3	N	TA	−1, −5, −10, −20	0.3–2	–		Sand	–	ϕ40 × 80	2.64	33.04	–	–	–	–	–
38	Zhao et al., 2020	Stress path	Y	TA (MTS-810)	−6	–	–	–	Loess	–	ϕ62 × 125	–	30	2.07	28.8	15.7	–	–
39	Shastri et al., 2021	T, loading type, σ_3	Y	–	−6 ~ −26	0–54.6	10×10^{-4}	–	Silty clay	Alaska	–	–	40	1–1.3	–	–	–	–
40	Shen et al., 2021	Stress path	Y	TA (MTS-810)	−6	–	–	–	Loess	China (Lanzhou)	ϕ61.8 × 125	–	16	1.782	27.14	18.33	–	–
41	He et al., 2023b	σ_3	N	TA (MTS Landmark 370.10)	−6	0.2–1.2	1.67×10^{-4}	–	Red-bed weathered soil	China (Qinghai Province)	ϕ61.8 × 125	–	13	1.528	–	–	–	–
42	Huang et al., 2022	Intermediate principal stress*	N	True TA	−10	0.8–2.6	–	–	Sand		100 × 100 × 100	–	12	–	–	–	–	–
43	Qu et al., 2022	FTC	N	–	−20	0.15	–	Cycles = 4, 7, 11, T_t = 20 °C	Silty clay	China (Heilongjiang Province)	ϕ61.5 × 121	–	22.38	1.47	–	–	–	–
44	Yu et al., 2022	FTC, T	N	TA	−5, −10, −15	0.2	–	Cycles = 0, 5, 10, 20, 30, T_t = 30 °C	Silty sand		ϕ39.1 × 80	–	12.2	1.97	25.6	17.6	–	–
45	Wang et al., 2023a	FTC, f_c, σ_3	Y	–	−10	0.3, 1.4	1.67×10^{-4}	Cycles = 0, 5, 10	Clay with coarse-grained gravel	China (Qinghai–Tibet Railway)	ϕ61.8 × 125	–	16.8	1.89	27.5	15.9	–	0, 30

Notes: ε_v is volumetric strain; T is temperature; T_t is thaw temperature; σ_3 is confining pressure; $\dot{\varepsilon}$ is axial strain rate; FTC is freeze-thaw cycles test; G_S is specific gravity; ω is initial water content; LL and PL are liquid limit and plastic limit; f_s is salt content; f_c is the coarse grains content; TA is triaxial apparatus; Y and N represent yes and no, respectively. MTS is material testing system; ϕ is diameter. * indicates that the intermediate principal stress ratio b = 0.2, 0.4, 0.6, 0.8, 1.

Table 2
Summary of uniaxial compression tests on frozen soils.

No.	Refs.	Test conditions					Frozen soil samples								
		Influence factors	Device	T (°C)	$\dot{\varepsilon}$ (/s)	FTC	Types	Locations	Size (mm)	G_s	ω (%)	ρ_{dry} (g/cm^3)	LL (%)	PL (%)	f_s (%)
1	Ogata et al., 1983	T, f_s, soil type	TA	−32, −20, −10, −2	1.7×10^{-4}	–	Sand and cohesive soil (alluvial sand, clayed silt and kaoline)	Japan	ϕ50 × 100	–	–	–	–	–	0, 0.5, 1, 1.5, 2, 3
2	Zhu and Carbee, 1984	T, $\dot{\varepsilon}$, ρ_{dry}	TA	−0.5, −1, −2, −3, −5, −7, −10	5.5×10^{-2}, ~ 1.1×10^{-6}	–	Silt	US (Alaska)	ϕ70 × 152	2.68	–	(1.08–1.10), (1.18–1.23), (1.39–1.43)	38.4	34.2	–
3	Pharr and Merwin, 1985	T, f_s	TA	−15.5 ~ −2.5	10^{-4}	–	–	–	ϕ50.8 × 108	–	20	16.8	–	–	0, 1.6, 3.2, 4.8
4	Hivon and Sego, 1995	T, f_s, soil type	TA	− 12, − 10, −7, −5	2×10^{-6}	–	Fine sand, silty sand, Devon silt	–		2.67	17.4, 16.6, 22.2	–	–	–	0, 0.05, 0.1, 0.3
5	Li et al., 2001	T, $\dot{\varepsilon}$	Low-temperature apparatus	−15	–	–	Silty sand	–	100 × 100 × 300	–	–	–	–	–	–
6	Li et al., 2024a, b	T, $\dot{\varepsilon}$, ρ_{dry}	TA	−2, −5, −10, −15	1.067×10^{-6}–6.67×10^{-4}	–	Clay	–	ϕ61.8 × 150	–	34, 25.4, 16	1.38, 1.58, 1.88	28.8	17.7	
7	Christ et al., 2009	T, FTC, soil type	Standard compression testing equipment	−2, −5, −10	1.67×10^{-4}	Cycles = (0,10), (0, 5, 10, 20), (0, 5, 10, 20); T_t = −1 °C, T_f = −10 °C	Sand, silty sand, silt	–	ϕ50 × 100	–	11.9, 11.7, 19.8	1.9, 1.91, 1.53	–	–	–
8	Liu and Peng, 2009	T, ω	TA (SLB-1)	−10, −5, −3	1.11×10^{-5}	–	Sandy soil	China (Beijing–Baotou–Lanzhou railway)	ϕ100 × 150	2.663	13, 15, 18, 20, 23	1.87	30	20.1	–
9	Nguyen et al., 2010	T, $\dot{\varepsilon}$, $\boldsymbol{f_s}$	TA	−2, −4, −6, −10	1.67×10^{-4}, 1.67×10^{-5}, 1.67×10^{-6}	–	Sands	–	ϕ63.5 × 127	2.65	37	–	–	–	5, 13, 20 g/L NaCl
10	Yang et al., 2015	T, ρ_{dry}, ω	Universal testing machine (UTM-100)	−0.7 ~ −11.6	10^{-3}	–	Sandy organic silt, silt	US (Alaska)	–	2.44, 2.55	86–225, 63–134	320–780, 534–941	47, 39	44, 37	–
11	Xu et al., 2017b	T, σ_3, $\dot{\varepsilon}$	–	(−2, −4, −5, −7), −4	1.67×10^{-4}, (10^{-2}, 10^{-3}, 10^{-4}, 5×10^{-5}, 10^{-5})	–	Loess (silty sand)	China (Inner Mongolia Province)	ϕ61.8 × 125	2.526	23.58	1.97	–	–	–
12	Fei and Yang, 2019	T, $\dot{\varepsilon}$, ρ_{dry}, ω	–	−0.5 ~ −10	1.1×10^{-6}, 1.1×10^{-5}, 1.1×10^{-4}, 1.1 × 10−3, 5.6×10^{-3}, 6×10^{-2}	–	Silt	Alaska (Fairbanks)	ϕ70 × 152	2.68	47.7–51.2, 39.4–45.9, 30.3–31.7	1.08–1.12, 1.155–1.239, 1.309–1.426	34	38	–

(*continued on next page*)

Table 2 (*continued*)

13	Girgis et al., 2020	T, $\dot{\varepsilon}$, soil type	–	0, −0.5, −1, −2, −5, −10, −15	1.64×10^{-4}, 4.92×10^{-4}, 1.48×10^{-3}	–	Sandy clay (Kaolinite-sand, Bentonite sand)	–	ϕ50.8 × 101.6	2.65, 2.63	23, 59	1.76, 1.53	30, 97	20, 34	–
14	Kotov and Stanilovskaya, 2021	Soil type, T, ω, f_s	–	−2, −4, −6	–	–	Clay, loam, fine sand	–	ϕ40 × 80, ϕ75 × 35	2.73, 2.71, 2.66	26/46; 20/30; 10/24	1.75/1.63; 1.89/1.78; 1.93/1.82	45, 31, –	25, 20, –	0.19, 0.5, 1.03; 0.19, 0.51/0.52, 1.02/1.05; 0.04, 0.52/0.54, 1.05/1.01
15	Yang et al., 2022	FTC, ω	–	−10	–	Cycles = 0, 1, 3, 5, 7; T_t = 30 °C	Weak expansive soil	China (Shandong Province)	ϕ61.8 × 125	2.73	18.2, 20.2, 22.2, 24.2	1.53	44.6	22.7	–
16	Zhang et al., 2022	T, σ_3	MTS 370.25	−5, −7, −10, −15, −20	1.67×10^{-4}	–	Silt	China	ϕ50 × 100	–	25.5	–	–	–	–
17	Ren et al., 2023a	T, ω	WDW-100 low-temperature electronic universal testing machine	−5, −10, −20, −30, −40, −50, −60, −70, −80	8×10^{-4}	–	Clay	–	ϕ61.8 × 125	–	17, 20, 23	1.7	36.5	17.5	–
18	Shi et al., 2023b	Structural type (with ice lens inclination angle = 60°, thickness = 10 mm), T	–	−1, −2, −3, −4, −5	1.04×10^{-4}	–	Clay	Northeast China	100 × 90 × 20	2.75	–	1.7	37	25	–

Notes: T is temperature; σ_3 is confining pressure; $\dot{\varepsilon}$ is axial strain rate; FTC is freeze-thaw cycles test; G_S is specific gravity; ω is initial water content; ρ_{dry} is dry density; LL and PL are liquid limit and plastic limit; f_s is salt content; TA is triaxial apparatus; MTS is material testing system; ϕ is diameter.

Table 3
Summary of creep tests on frozen soils.

No.	Refs.	Test conditions							Frozen soil samples								
		Factors	Tests	Devices	t_c	T (°C)	Stress (MPa)	FTC	Types	Locations	Size (mm)	G_S	ω (%)	ρ_{dry} (g/cm^3)	LL (%)	PL (%)	f_c (%)
1	Alkire and Andersland, 1973	σ_3	TCT	TA	400 min	−12	–	–	Silica Ottawa sand	–	ϕ28.7 × 57.4		–	–	–	–	–
2	Sayles, 1974	σ_3, $\dot{\varepsilon}$	TCT	TA	120 h	−3.85	0.525–6.89	–	Ottawa sand	–	ϕ70 × 152.5	2.65	18.8–25.1	1.67	–	–	–
3	Orth, 1986	Stress level	UCT	–	2000 min	−2, −5, −10, −15	1–14	–	Karlsruhe medium sand	–	ϕ100 × 100	2.65	18	–	–	–	–
4	Yang et al., 2010a	Stress level	UCT	TA (MTS-810)	24 h	−1, −1.5, −2	0.5–1.01	–	Sand	China (Qinghai–Tibet Railway)	ϕ61.8 × 125	–	30	1.43	–	–	–
5	Li et al., 2011	T, σ_3	TCT	TA (Self-developed W3Z-200)	24 h	−5, −10, −15, −20, −25,	–	–	Clay	China	ϕ61.8 × 150	–	29	–	77.6	38.4	–
6	Zhao and Zhou, 2013	Thermal gradient (0 °C/cm, 0.25 °C/cm, 0.5 °C/cm)	UCT	TA	100 h	−20	2.55–4.58	–	Clay	–	ϕ100 × 200	–	33.59	1.42	23.67	51.88	–
7	Hou et al., 2018	σ_3	TCT	TA (MTS-810)	24 h	−10	3.21–6.52	–	Silty clay with quartz sand (100:60)	–	ϕ61.8 × 125	2.72, 2.66	1.35, –	–	27.58, –	19.37, –	–
8	Zhou et al., 2016	Stress level	TCT	TA	24 h	−3, −6, −9	1–5	–	Frozen loess	China (Lanzhou)	ϕ62 × 125	–	16.5	1.78	–	–	–
9	Li et al., 2017	T, σ_3	TCT	TA (W3Z-200)	24 h	−5, −10, −15, −20	0.3, 0.5, 0.7 strength	–	Clay	–	ϕ61.8 × 125	–	–	–	–	–	–
10	Liao et al., 2017	Stress level, σ_3	TCT	TA (MTS-810)	20 h	−1.5	(0.79–1.843), (0.272–1.940), (0.642–1.498)	–	Warm frozen silt	China (Qinghai–Tibet Railway)	ϕ61.8 × 125		15.8	1.8	–	–	–
11	Hou et al., 2018	Coarse grains content	TCT	TA (MTS-810)	24 h	−10	–	–	Silty clay mixed with coarse grains	–	ϕ61.8 × 125	2.72, 2.66	1.35, 0	–	27.58	19.37	0, 20, 40, 60
12	Zhou et al., 2018	FTC, σ_3	TCT	TA (MTS-810)	24 h	−6, −12	–	Cycles = 0, 3, 6, 9, 12; T_t = 15 °C	Loess	China (Lanzhou)	ϕ62 × 125	–	–	–	17.4	25.7	–
13	Zhu et al., 2019a	ρ_{dry}, grain size distributions*	TCT	TA (MTS-370.10)	< 20	−0.5, −0.9, −1.2, −1.5, −2	–	–	Sand	China (Qinghai–Tibet Railway)	ϕ61.8 × 125	–	15.6	1.75, 1.92	–	–	–
14	Li et al., 2020c	T, σ_3	TCT	TA (self-developed W3Z-200	24 h	−5, −10, −15	–	–	Clay	China (Huainan)	ϕ61.8 × 125	–	–	–	–	–	–

(*continued on next page*)

Table 3 (*continued*)

No.	Refs.	Test conditions							Frozen soil samples								
		Factors	Tests	Devices	t_c	T (°C)	Stress (MPa)	FTC	Types	Locations	Size (mm)	G_S	ω (%)	ρ_{dry} (g/cm^3)	LL (%)	PL (%)	f_c (%)
				testing system)													
15	Li et al., 2020b	FTC	TCT	TSS10 triaxial creep test system	100 h	−10, −20, −30	–	–	Clay	China (Shanghai)	ϕ39.1 × 80	2.74	47.1	1.16	–	–	–
16	Zhou et al., 2021	Consolidation pressure, stress path	TCT	TA (MTS-810)	24 h	−6	–	–	Loess	–	ϕ62 × 125	–	30	2.07	28.8	15.7	–
17	Wang et al., 2022	Stress level, constant/variable T	TCT	–	24 h	−4, −1.5, −0.5	0.345–1.216	–	Silty clay	western China	ϕ61.8 × 125	–	7.23	1.7	28.5	17.4	–
18	Zhang et al., 2022	T, σ_3	TCT	TA (MTS 370.25)	12 h	−5, −7, −10, −15, −20	0.79–3.7	–	Silt	China	ϕ50 × 100	–	25.5	–	–	–	–
19	Schindler et al., 2023	Loading history	UCT	–	2000 min	−4.3	–	–	Sand		ϕ50 × 100	2.65	20	1.66	–	–	–
20	Shen et al., 2023	Pressure history, stress path	TCT	TA (MTS-810)	24 h	−6	–	–	Clay	China (Lanzhou)	ϕ61.8 × 125	2.72	16	1.769	27.17	14.15	–
21	Shi et al., 2023a	Deviatoric stress, heterogeneous soil structure	TCT	GDS frozen soil triaxial testing machine	5 h	−2	0.1, 0.4, 0.7, 1	–	Clay	Northeast China	ϕ200 × 100	–	–	–	–	–	–

Notes: ε_v is volumetric strain; t_c is creep time; T is temperature; FTC is freeze-thaw cycles test; LUC is loading-unloading cycles test; G_S is specific gravity; ω is initial water content; LL and PL are liquid limit and plastic limit; f_s is salt content; f_c is the coarse grains content; σ_3 is confining pressure; $\dot{\varepsilon}$ is axial strain rate; TCT is triaxial creep test; UCT is uniaxial creep test; MTS is material testing system; ϕ is diameter; * represents that three different content were considered in Zhu et al. (2019a) tests where the content of particle with 0.075 to 1 mm were 0.54, 0.6 and 0.69.

Table 4
Summary of other experimental tests on frozen soils.

No.	Refs.	Test conditions							Frozen soil samples							
		Factors	Tests	Devices	T (°C)	Stress (MPa)	$\dot{\varepsilon}$ (/s)	FTC	Types	Locations	Size (mm)	G_S	ω (%)	ρ_{dry} (g/cm^3)	LL (%)	PL (%)
1	Azmatch et al., 2011	T, $\dot{\varepsilon}$	Four-point bending test	–	−0.3 ~ −1.4	–	–	–	Devon silt	–	304.8 × 76.2 × 76.2	2.65	27	–	32	22
2	Zhou et al., 2018	FTC, σ_3	Stress relaxation tests	TA (MTS-810)	−6, −12	–	–	Cycles = 0, 3, 6, 9, 12; T_t = 15 °C	Loess	China (Lanzhou)	ϕ62 × 125	–	–	–	17.4	25.7
3	Chen et al., 2019	θ = −30°, −16.1°, 0°, 16.1°, 30°, p	Directional shear test	Dynamic hollow cylinder apparatus	−6, −10, −15	1, 3, 4.5, 10	–	–	Clay	China (Qinghai–Tibet Railway)	ϕ60/100 (I/O) × 125	–	19.8	1.9	–	–
4	Wang et al., 2019a	T, $\dot{\varepsilon}$	Small-strain loading test	TA	−2, −5, −10	–	1.67× 10–5, 1.67× 10^{-6}, 1.67× 10^{-7}	–	Kasaoka clay	Japan	ϕ30 × 60	–	–	–	59.6	22.5
5	Girgis et al., 2020	T, $\dot{\varepsilon}$	Step-loaded relaxation test	–	−1, −5, −10, −15	–	1.64 × 10^{-4}, 1.48 × 10^{-3}	–	Sandy clay (Kaolinite-sand, bentonite sand)	–	ϕ50.8 × 101.6	2.65, 2.63	23, 59	1.76, 1.53	30, 97	20, 34
6	Zhou et al., 2020	Consolidation pressure, stress path	Stress relaxation test	TA (MTS-810)	−6	–	–	–	Loess	–	ϕ62 × 125	–	30	2.07	28.8	15.7
7	Chen et al., 2022	Principal stress directions, anisotropy	Directional shear test	Hollow cylinder apparatus	−10	2, 4.5, 6	–	–	Standard sand	China	ϕ100/60 ((I/O) × 200	2.643	1,53	–	–	–
8	Chang et al., 2023	T, normal pressures (0.2, 0.4, 0.6, 0.8)	Large-scale direct shear test (shear rate = 2 mm/min)	Temperature-controlled large-scale direct shear apparatus (Txtzj-500)	−2, −5	–	–	–	Sand	–	ϕ50, variable length	2.65	8		–	–
9	Nishimura et al., 2023	Pre-freezing consolidation effective stress and total radial stress	Direct tension test	TA	−1,−4, −9, −15	–	−8.33 × 10^{-6}	–	Kasaoka clay	–	ϕ50/30 ((I/O) × 100	2.65	–	–	28	62

Notes: T is temperature; σ_3 is confining pressure; $\dot{\varepsilon}$ is axial strain rate; FTC is freeze-thaw cycles test; G_S is specific gravity; ω is initial water content; ρ_{dry} is dry density; LL and PL are liquid limit and plastic limit; TA is triaxial apparatus; MTS is material testing system; ϕ is diameter; θ is stress Lode angle; p is mean principal stresses.

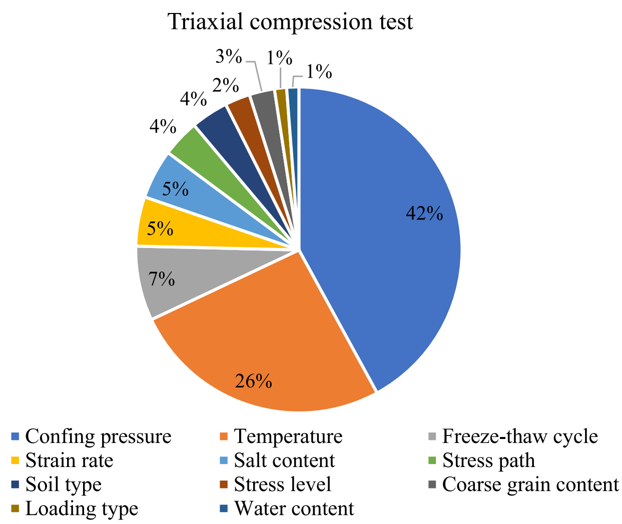

(a)

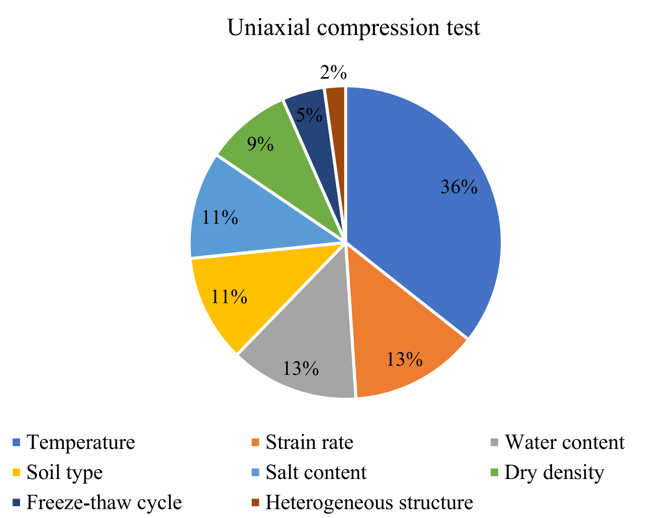

(b)

Fig. 3. Numbers of experimental studies on frozen soils with different influencing factors; (a) triaxial compression test; (b) uniaxial compression test; Note: This figure is based on the studies reviewed in this work.

2.2.1. Strength characteristics of frozen soils

The strength of frozen soils is a key parameter often defined as the peak stress observed during uniaxial or triaxial compression tests. It is influenced by several factors:

(1) Temperature: Experimental studies consistently show that the strength of frozen soils increases as temperature decreases. Lower temperatures enhance ice-particle bonding, leading to greater cohesion and stiffness. However, this also makes the soil more brittle, resulting in a sudden and catastrophic failure under high stress. The transition from ductile to brittle behavior is a critical aspect of frozen soil mechanics.

(2) Confining pressure: Confining pressure affects the strength and deformation behavior of frozen soils in two opposing ways. Higher confining pressure increases the frictional resistance between soil particles, enhancing strength. However, at very high confining pressures, ice melting and particle crushing occur, weakening the soil structure. This dual effect leads to a nonlinear relationship between strength and confining pressure, with a peak strength reached at a critical pressure.

(3) Moisture content and ice content: The moisture content of frozen soils directly influences the amount of ice present, which in turn affects strength. Higher ice content typically correlates with higher strength due to increased ice-particle bonding. However, excessive ice can lead to structural instability, especially under stress, as ice deformation dominates the mechanical response.

(4) Strain rate: The mechanical response of frozen soils is strain rate-dependent. At higher strain rates, frozen soils exhibit greater strength and stiffness due to the limited time for ice and unfrozen water to deform. Conversely, at lower strain rates, the soil exhibits softer, more ductile behavior as ice and water have sufficient time to redistribute under the applied load.

(5) Salinity: Saline frozen soils exhibit reduced strength compared to non-saline frozen soils due to the presence of unfrozen water at subzero temperatures. Higher salinity lowers the freezing point of water, resulting in a weaker ice matrix and reduced bonding between soil particles.

(6) Freeze-thaw cycles: Strength decreases with an increasing number of freeze-thaw cycles due to the expansion and contraction of ice, which generates microcracks and disrupts the soil structure. The degradation stabilizes after a certain number of cycles as the soil reaches a new equilibrium state. Besides, coarse-grained soils are generally more resistant to freeze-thaw degradation than fine-grained soils, as the larger particles provide greater structural stability.

2.2.2. Deformation and failure

Under static loading, the deformation behavior of frozen soils is governed by the interaction between soil particles, ice, and unfrozen water. The stress-strain response typically exhibits strain-softening or strain-hardening behavior depending on the soil type, ice content, temperature, and confining pressure (σ_3). These mechanical responses can be classified into five categories by (Zhang et al., 2007): strong strain hardening, weak strain hardening, strong strain softening, weak strain softening, and perfect plasticity.

(1) Strain Hardening: Strain hardening is most pronounced at higher confining pressures (typically above 3 MPa), where particle rearrangement is restricted, and at lower temperatures, which enhance ice bonding and structural stability. The degree of hardening varies among soil types. For instance, frozen saline sand and frozen silt exhibit a transition from weak to strong strain hardening as σ_3 increases (Yang et al., 2016). However, due to the weakening effect of salinity on ice bonding, frozen saline sand experiences delayed hardening, which only becomes significant when σ_3 exceeds 5 MPa (Lai et al., 2016). In contrast, frozen clay, characterized by high plasticity and strong interparticle cohesion, exhibits quasi-perfect plasticity with minimal strain hardening (Wang et al., 2017).

(2) Strain-softening: Strain softening is more pronounced at lower confining pressures, where particle sliding and ice bond degradation dictate the mechanical response. Frozen sand experiences significant post-peak strength loss under these conditions (Xu et al., 2016), particularly at lower temperatures, where initial ice bonding temporarily enhances strength but ultimately leads to brittle failure upon bond breakage. Similarly, frozen silty clay undergoes progressive strain softening at low σ_3 and low temperatures due to structural degradation (Xu et al., 2020a,b). Frozen saline sand is also highly susceptible to softening, as salinity weakens ice bonding, making it more prone to post-peak strength loss. In contrast, frozen clay exhibits only limited strain softening, as its intrinsic cohesion helps maintain structural integrity even after reaching peak strength (Wang et al., 2017).

(3) Failure modes: The failure modes of frozen soils vary with loading conditions and environmental factors. Brittle failure is commonly observed at lower temperatures and higher strain rates, while ductile deformation occurs at higher temperatures and lower strain rates. The presence of ice lenses and heterogeneities in the soil structure can also lead to localized failure and stress concentration.

Table 5
Summary of typical mechanical behaviors of frozen soils under different influencing factors.

Influencing factors	Frozen soils	Static tests	Mechanical behaviors	Primary characteristics	References
Confining pressures (σ_3)	Silt	Triaxial compression test	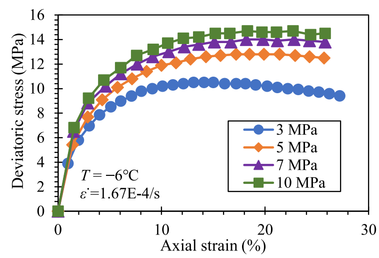 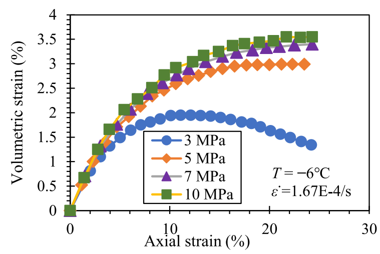	(1) The strength increases with increasing σ_3 at first, but the strength decreases with further increments in σ_3 due to pressure melting and crushing phenomena under high σ_3. (2) The frozen silt exhibits strain softening at low confining pressures, while the frozen silt presents strain hardening at high confining pressures.	Lai et al., 2010a
Temperature (T)	Sand	Triaxial compression test	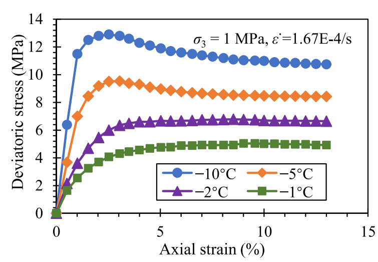 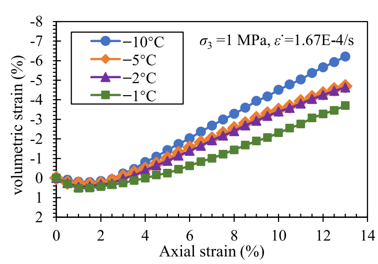	(1) The strength increases as T decreases due to the enhanced cementation of ice. (2) The volumetric strain increases with decreasing T, which is attributed to the transition of the specimen from a plastic to a brittle nature.	Xu et al., 2016
Strain rate ($\dot{\varepsilon}$)	Silt	Uniaxial compression test	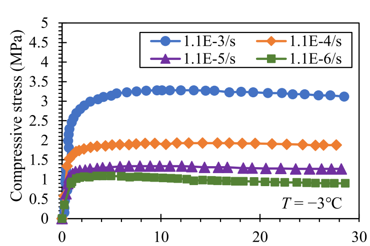	(1) Strain softening; (2) The strength increases with the increment of strain rate.	Zhu and Carbee, 1984

(continued on next page)

Table 5 (*continued*)

Influencing factors	Frozen soils	Static tests	Mechanical behaviors	Primary characteristics	References
Freeze-thaw cycles	Expansive soils	Triaxial compression test	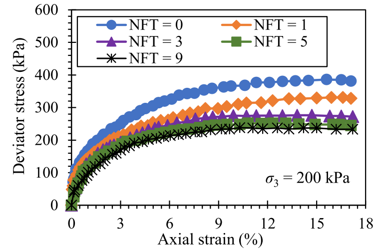	(1) The strength decreases as the freeze-thaw cycles (NFT) increase; (2) The frozen expensive soils display the strain-softening with increasing σ_3. Besides, the mechanical properties become stable once the freeze-thaw cycles exceed a threshold value (i.e., NFT = 5).	Tang et al., 2018
Salt content	Coarse sandy soil	Triaxial compression test	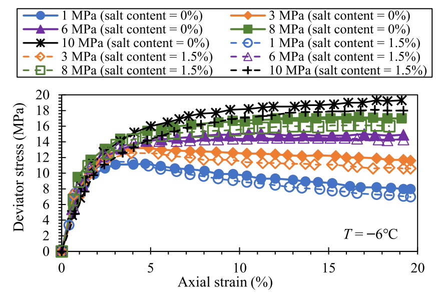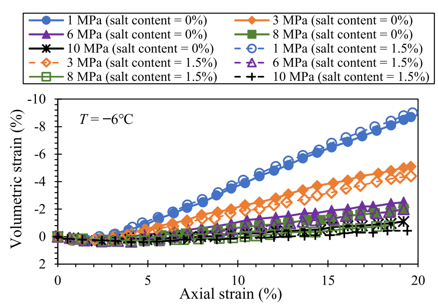	The strength decreases with the increase in salt content since higher salinity causes an increment in unfrozen water content, consequently reducing strength.	Chang et al., 2019
Dry density	Silt	Uniaxial compression test	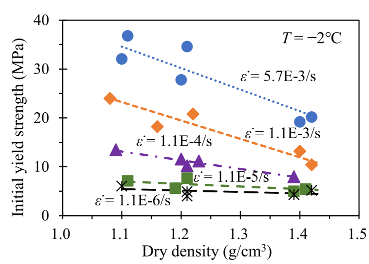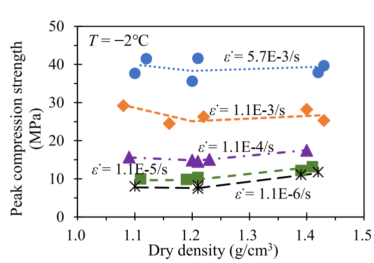	(1) The initial yield strength decreases with increasing dry density. (2) The peak strength appears to be less influenced by dry density, especially at high strain rates. At high strain rates, the peak strength remains relatively constant across various dry density levels. However, at low strain rates, the peak strength for low density is lower than that for high dry density due to the enhanced rheological properties of the ice matrix.	Zhu and Carbee, 1984

(*continued on next page*)

Table 5 (*continued*)

Influencing factors	Frozen soils	Static tests	Mechanical behaviors	Primary characteristics	References
Water content	Silt clay	Triaxial compression test	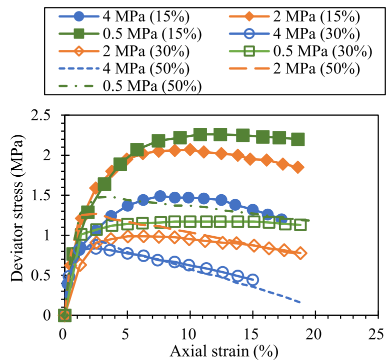 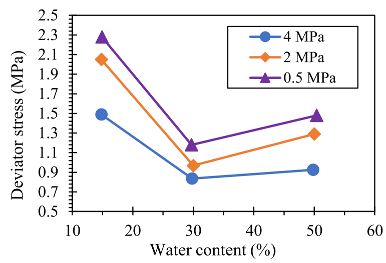	(1) Strain-softening; (2) The strength initially decreases as the water content increases but then shows a subsequent increase.	Zhang et al., 2020a
Coarse-grained content	Silty clay with coarse sand	Triaxial compression test	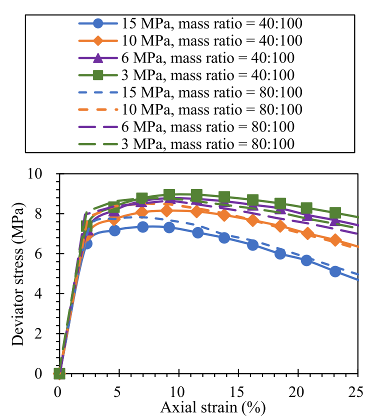 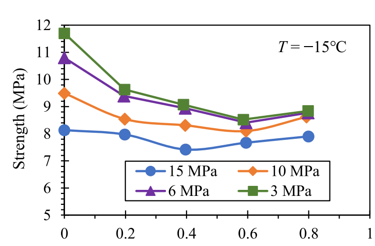	(1) Strain-softening; (2) The strength consists of the bond strength between ice and the friction between particles. As the coarse grain content increases, the water and ice content in the frozen samples decrease, reducing ice bond strength. Additionally, an increase in the mass ratio results in a higher content of coarse particles and an increase in the frictional force between particles. Consequently, the strength of frozen mixed soil samples generally exhibits an initial decrease followed by an increase with an increasing mass ratio. This behavior can be attributed to the dominant effect of decreasing ice-cemented force on strength at low mass ratios. In contrast, the increasing frictional force among inner particles becomes more significant at high mass ratios.	Liu et al., 2019

(*continued on next page*)

Table 5 (*continued*)

Influencing factors	Frozen soils	Static tests	Mechanical behaviors	Primary characteristics	References
Heterogeneous structures	Clay	Uniaxial compression test	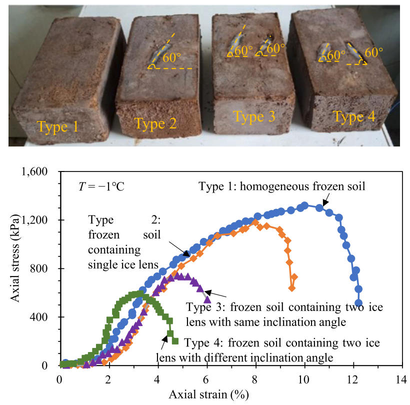	(1) Strain-softening; (2) The order of uniaxial compression strength is Type 1 > Type 2 > Type 3 > Type 4 frozen soil. The strength decreases with an increasing number of ice lenses, particularly for Type 4 frozen soil. This can be attributed to the ice lenses cutting through the frozen soil destroying its integrity. Besides, the presence of ice lenses promotes stress concentration at their tips during loading, which further exacerbates the failure of the frozen soil.	Shi et al., 2023b

Notes: The aforementioned figures on the mechanical behaviors of frozen soils are modified from corresponding references.

2.2.3. *Creep*

The creep is one of the most vital aspects of the time-dependent behaviors of frozen soils. Due to the viscosity of ice and water, frozen soils possess significant creep deformation properties under external load conditions (Ladanyi, 1972; Wang et al., 2019b). The creep deformation has been acknowledged as one of the essential sources of uneven settlement and hazards in permafrost regions (Yu et al., 2013; Xu et al., 2017c) and is closely related to ground temperature (Mu et al., 2020).

The creep deformation of frozen soils is affected by many factors, such as temperature, stress level and state, moisture content, ice content, soil types, and so on (Ladanyi, 1972; Andersland and Ladanyi, 2003; Zhou et al., 2016; Zhu et al., 2019a; Wang et al., 2020b). Existing experimental studies have indicated that the characteristics of creep deformation possess two types: attenuation creep and nonattenuation creep (see Fig. 4). The attenuation creep occurs when the shear stress is less than the long-term strength, where the creep rate gradually decreases and ultimately remains constant (i.e., the curve $OA_1A_2A_3$ in Fig. 4), and this creep deformation increases as deviatoric stress rises. In contrast, the creep curve becomes non-attenuated when the shear stress exceeds the long-term strength, including three stages: decaying creep (also named primary creep), steady creep (also called secondary creep), and accelerated stage (also termed tertiary creep). During the primary creep, ice-hardening controls the behaviors of frozen soil, leading to a decreasing creep rate. As for the secondary creep, the creep rate is constant and keeps its minimum values, and the frozen soil exhibits its maximum creep resistance. During the tertiary stage, where the creep rate gradually increases until the failure of frozen soil, cracking of the ice matrix becomes more dominant than ice-hardening, and excessive deformation occurs within a short period, which can result in damage to infrastructure such as pipelines, foundations, and railways (Sun et al., 2020). Since the frozen soil in deep alluvium withstands considerable ground pressure and is prone to enter the accelerated stage, this stage should be considered (Li et al., 2020c).

The creep of frozen soils was also investigated via scanning technologies (e.g., computed tomography (CT)) that observed the change of internal structure during the creep process (Wu et al., 1995; Ma et al., 1997; Torrance et al., 2008; Li et al., 2020b). Specifically, both the pore volume and accumulated area decreased, and the size distribution became more evenly after creep due to the pore closure caused by soil compression and pores gathering larger pores (Li et al., 2020b). These phenomena were also observed in the CT scanning tests by Wu et al. (1995) (see Fig. 5). As a typical three-phase material, the creep deformation stems from the collective contribution of each component and their individual properties (Li et al., 2019). On the one hand, the viscosity of ice, unfrozen water and soil fabric enhance the creep properties of frozen soils. On the other hand, the pore ice in the frozen soils is likely to be partially melted and crushed by stress concentration, which in turn results in the weakening of ice-cementation and increment of unfrozen water content, facilitating the readjustment of solid particle displacement (Li and He, 2024).

Besides, given the application of AGF in tunnel excavations, varying stress states and different loading types exist during the construction

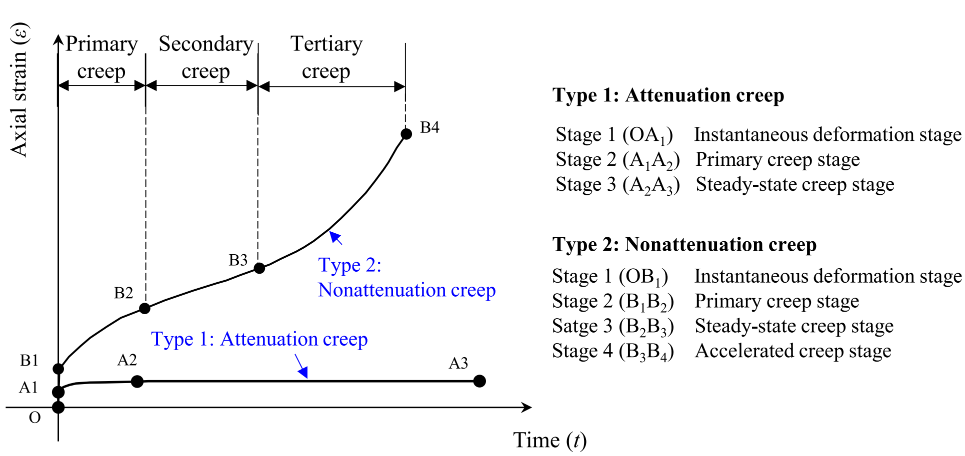

Fig. 4. Typical creep curves of frozen soils (modified from He et al., 2023a).

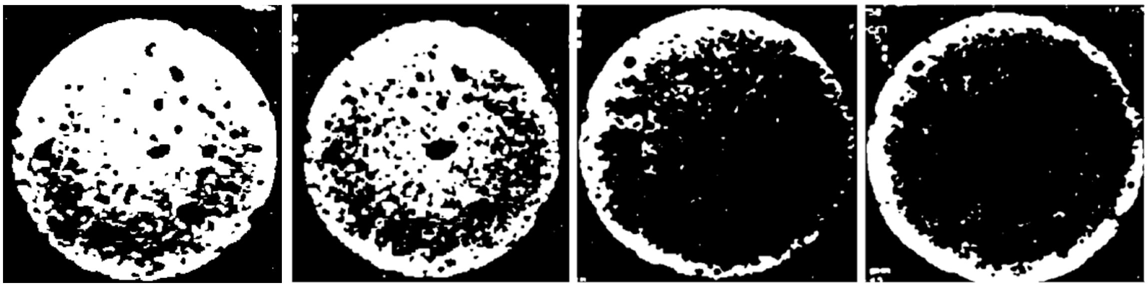

Fig. 5. CT images of frozen soils at different creep stages (modified from Wu et al., 1995; Yang et al., 2010a).

stage, resulting in the shearing of frozen soils and rapid increases in stress. The excavation leads to the shearing of the frozen soil and a relatively rapid growth in stress. After tunnel excavation, the frozen soil body undergoes deformation under a predominantly constant stress state and needs to provide support until the tunnel lining is finished. Common excavation techniques (e.g., partial face advance) can cause a stepwise increment in loading of the frozen soil body, and the duration of stepwise increased loading could be up to over six months. For insurance, three long-duration excavation steps during the challenging construction of the Toledo underground station in Italy were documented by Russo et al. (2015). Some scholars (i.e., Classen et al., 2019; Zhou et al., 2021) explored the usage of AGF to support large-scale tunnel excavations with fourteen excavation stages. On the other hand, the unloading state of frozen soils during construction may result from complex stress histories, including repeated loading and unloading, which influence the mechanical response. The unloading creep behaviors of frozen soil are rarely reported despite being the most realistic stress state in underground engineering. Therefore, these instances provide compelling evidence for the critical need to enhance the fundamental understanding of the impact of loading/unloading history and load path on the mechanical performances of frozen soils from a practical perspective. Some investigations (e.g., Vyalov et al., 1989; Zhou et al., 2021) have been conducted, and their results contributed to the understanding of the complex mechanical behaviors of frozen soils, which is dependent on the strain-strain history. In contrast, Schindler et al. (2023) concluded via uniaxial single-stage and multi-stage loading tests that both the average axial strain at the turning point (i.e., the moment when the tertiary begins) and the minimum strain rate are independent of load history. They also proposed a transform creep time to convert the multi-stage creep tests into single-stage tests. Therefore, further investigations involving broader loading and creep stages are necessary to reinforce the loading history independence. Largely, the impacts of the stress and strain history (e.g., stepwise loading) on the rate-, stress-, and temperature-dependent mechanical behavior of frozen soils is not yet fully comprehended, which is crucial for safe construction and maintenance in geotechnical engineering, particularly in controlling deformation and preventing hazards in the artificially frozen ground.

3. Mechanical behaviors under dynamic loading

3.1. Experimental methodology

Up to now, investigations on the dynamic responses of frozen soils for practical engineering applications remain a challenging task, primarily due to the limited availability of testing equipment capable of exploring the dynamic behavior of frozen soils, such as the split Hopkinson pressure bar (SHPB) and some other specialized devices (such as frozen hollow cylinder apparatus and bender elements). Furthermore, the complex environment and other soil properties (e.g., temperature, strain rate, and water content) can affect the mechanical behaviors of frozen soils under dynamic loadings.

The SHPB method has emerged as an efficient tool for dynamic testing for various materials under high strain rates (10–10,000/s) related to engineering applications such as seismic actions, vibration, and blasting loadings (Ma et al., 2019), which was initially applied for metals and then developed for exploring other construction materials (e.g., rock and concrete). The US Sandia National Laboratory first examined its application for frozen soils (Furnish, 1998). They conducted experiments on artificially frozen soils from Alaska, subjecting them to uniaxial strain conditions or negative lateral confinement. Their results revealed that the Alaskan frozen soils depend on both pressure and temperature, in addition to displaying characteristics such as rate sensitivity, anisotropy, and brittle and ductile behaviors. Subsequently, Lee et al. (2002) extended their investigations to undisturbed frozen soils and introduced a cap plasticity model to characterize the dynamic mechanical responses. However, the results exhibited significant differences in the observed behavior, primarily attributed to undisturbed frozen soils' inherent heterogeneity and complexity. Consequently, their proposed model is too complex and fails to accurately capture frozen soils' dynamic behaviors. Based on the principles of one-dimensional stress wave theory (Kolsky, 1949) and the assumption of uniform stress, soil samples' strain rate, strain, and stress history can be deduced utilizing three signals (i.e., the incident, reflected, and transmitted) by the following equations.

$$\dot{\varepsilon}(\mathrm{t}) = -\frac{2\mathrm{C}_0}{\mathrm{l_s}}\varepsilon_\mathrm{r} \tag{1}$$

$$\varepsilon(\mathrm{t}) = -\frac{2\mathrm{C}_0}{\mathrm{l_s}}\int_0^t \varepsilon_\mathrm{r}\mathrm{dt} \tag{2}$$

$$\sigma(\mathrm{t}) = \frac{A}{A_\mathrm{s}}\mathrm{E}\varepsilon_\mathrm{t} \tag{3}$$

where l_s is specimen length, A_s and A are the initial cross-sectional areas of soil specimen and bar, respectively, E and C_0 are Young's modulus and elastic wave speed of the bars, respectively, ε_r is the reflected strains on the incident bar, and ε_t is the transmitted axial strain on the transmission bar. Once the three signals are measured, the stress-strain data of frozen soils can be determined. Fig. 6 shows schematic diagrams of the SHPB apparatus and three typical waves (i.e., incident, reflected, and transmitted). Liu et al. (2014) also designed an efficient temperature-controlled dynamic direct shear system that can be applied to various dynamic shearing loads and accurately control temperature for analyzing frozen soils' dynamic characteristics and interface properties.

Recently, the hollow cylinder apparatus (HCA) has emerged as a critical experimental tool for studying the mechanical behavior of frozen soils under complex stress conditions (see Table 6), especially in scenarios involving principal stress rotation, cyclic loading, and multi-stress-path environments. For example, Chen et al. (2022) conducted a series of tests on frozen soil to investigate the effects of principal stress direction on the anisotropic behavior and non-coaxiality. Liu et al. (2024a, 2024b) conducted a series of experiments using FHCA to simulate the cardioid-shaped stress path induced by repeated traffic

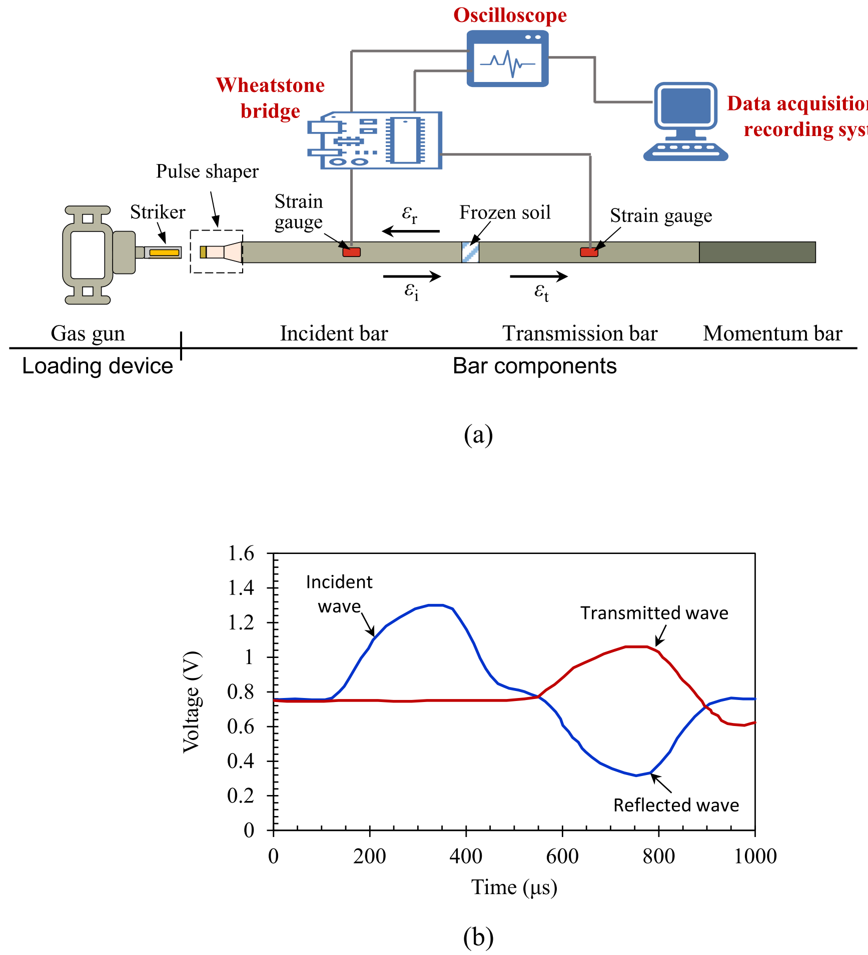

Fig. 6. Schematic diagram of (a) split Hopkinson pressure bar (SHPB) device; (b) three typical waves.

loads on frozen silt. Their results demonstrated that the rotation of the principal stress direction accelerates axial permanent deformation in frozen soil by increasing viscous energy dissipation. This study highlights the ability of HCA to capture the dynamic deformation behavior of frozen soils under complex stress paths, which conventional triaxial tests cannot replicate. Similarly, Liu et al. (2025) explored the dynamic responses of frozen soil under pure principal stress rotation (PSR) induced by wave loads using the FHCA. This capability of the HCA to simulate pure PSR conditions fills a critical gap in understanding wave load-induced deformation in permafrost regions, such as coastal engineering foundations within the Arctic Circle.

3.2. Dynamic behaviors under different factors

Fig. 7 summarizes the investigated influencing factors in the studies reviewed in this work. In general, most experiments have primarily addressed the effects of cryogenic temperature and strain rate on the dynamic behaviors of frozen soils. Typical impact loading results are plotted in Figs. 8(a-b), showing that the compressive strength exhibits a positive strain rate and negative temperature sensitivity. This phenomenon has been widely reported (e.g., Zhang et al., 2013; Ning et al., 2014; Xie et al., 2014; Zhu et al., 2016; Ma et al., 2017; Zhu et al., 2017; Cao et al., 2018; Fu et al., 2019a, 2019b, 2019c; Zhu et al., 2019b; Zhang et al., 2020b; Zhu et al., 2020; Fu et al., 2021; Zhang et al., 2021; Zhu et al., 2021a, 2021b; Chunyu et al., 2023). The dynamic stress-strain curves can be divided into three stages: elastic/viscoelastic stage, plastic stage, and failure stage (Zhu et al., 2021b; Li et al., 2022). Besides, the frozen soils also exhibit remarkable strain softening beyond the peak stress (Xie et al., 2014) and show brittle damage at high strain rates or low temperatures (Zhu et al., 2016). In addition, some researchers have investigated the mechanical behaviors under cyclic triaxial loading (Xu et al., 2015; Xu et al., 2020b). For example, Xu et al. (2020b) conducted a series of cyclic triaxial tests on frozen silty clay, and the corresponding mechanical responses are shown in Fig. 8(c). One can observe that the stress-strain curve exhibits hysteresis and a gradual accumulation of irreversible strains with increments in the number of cycles. Furthermore, the differences in residual axial strain between two adjacent cycles decrease in the initial loading cycles and then increase as the loading cycles progress.

In practice, frozen soils are often subjected to pre-existing stresses before impact loading, so it is crucial to explore the dynamic mechanical behavior of frozen soil under confining pressure. Accordingly, Ma et al. (2017) conducted a series of SHPB tests on frozen sandy clay under varying temperatures, strain rates, and confining pressure. The dynamic stress-strain of frozen soils reveals that the confining pressure has a negative effect on the dynamic strength of frozen sandy clay since the internal structure of frozen soils can be destroyed by high confining pressure. Subsequently, to study the coupled static and dynamic loads that are more in accordance with the actual loading conditions, Ma et al. (2019) employed a modified triaxial SHPB system developed by Central South University for dynamic impact tests; their experimental data revealed: (1) The dynamic compressive strength of frozen silty clay on the uniaxial and coupled static and dynamic states increases linearly with the logarithm of $\dot{\varepsilon}$; (2) The confining pressure has considerably enhanced the strength of frozen silty clay at coupled static and dynamic loadings, and their relations are nearly exponential; and (3) The frozen soil specimens subjected to axial pre-compressive state exhibited higher strength in comparison to those tested under uniaxial conditions.

Table 6
Summary of typical experimental investigations of frozen soils under dynamic loadings.

No.	Refs.	Test conditions					Frozen soil samples							
		Type	Device	T (°C)	Loading (Default: $\dot{\varepsilon}$/s)	σ_3 (MPa)	Type	Location	ρ_{dry} (g/cm^3)	ω (%)	LL (%)	PL (%	Size (mm)	Influence factors
1	Vinson et al., 1978	Cyclic DTC	Cyclic triaxial test system	−1, −4, −10	Axial strain amplitude = 2×10^{-3}–$8 \times 10^{-2\%}$	0–1.4	Clay	Michigan	1.09–1.52		40–98	23–37	ϕ100 × 200	Axial strain amplitude, soil type, T, σ_3, ω
2	Czajkowski and Vinson, 1980	Cyclic DTC	Cyclic triaxial test system	−1, −4, −10	Axial strain amplitude = 2×10^{-3}–$8 \times 10^{-2\%}$	0–1.4	Silt	Hanover, Alaska	–	35.5, 38.9	22, 28	-, 23	305 × 71 × 13	Axial strain amplitude, soil type, T, σ_3, ω
3	Lee et al., 2002	DTC	SHPB	−5, −10, −20	1000	–	Soil	Alaska	0.85–2.09	42			ϕ22 × 11	T
4	Ling et al., 2009	Cyclic DTC	Modified triaxial material test device (MTS-810)	−2, −5, −7, −10, −12	f = 6 HZ	0.5, 0.8, 1.0, 1.3	Clay	China (Beiluhe Basin)	1.8	13, 15, 18.19, 21, 23	39.3	20.8	ϕ61.8 × 120	T, σ_3, ω
5	Ling et al., 2013	Cyclic DTC	Modified triaxial material test device (MTS-810)	−0.5, −1	f = 2 HZ	0.3, 0.6, 0.9	Clay	China (Harbin–Daqing railway)	1.73	12, 16	26.7	12.5	ϕ61.8 × 125	T, σ_3, ω, and salt content (1.13 %, 3.42 %)
6	Zhang et al., 2013	Uniaxial strain and uniaxial stress test	SHPB	−3, −8, −13, −17, −23, −28	900–1500	–	Clay	China (Chengdu Province)	1.6	20	–	–	ϕ30 × 18	T, $\dot{\varepsilon}$
7	Ning et al., 2014	DUC	SHPB	−3, −13, −28	800–1400	–	Sand	–	1.7	15	–	–	ϕ45 × 21	T, $\dot{\varepsilon}$
8	Park and Lee, 2014	Elastic wave test	Piezo disk and bender elements	20 to −10	–	–	Sand–silt mixtures	Korea	–	–	–	–	100 × 100 × 200	T, saturation
9	Xie et al., 2014	DUC	SHPB	−3, −8, −18, −28	400–1000	–	Sand	–	1.6	30	–	–	ϕ30 × 18	T, $\dot{\varepsilon}$
10	Ling et al., 2015	Cyclic DTC	Modified triaxial material test device (MTS-810)	−2, −6, −10	f = 1, 2, 3, 4 HZ	0.3, 0.6, 0.9, 1.2	Clay	China (Heilongjiang Province)	2.01	8.63, 9.55, 10.7	–	–	ϕ61.8 × 125	T, σ_3, ω, f and F-T cycle (0, 1, 3, 5)
11	Liu et al., 2014	Cyclic DTC	Modified triaxial material test device (MTS-810)	−15	f = 1 HZ	0.6, 1.4, 6	Silty	China (Qinghai-Tibet Plateau)	1.848	8.86	32.3	18.3	ϕ61.8 × 125	σ_3, f
12	Zhu et al., 2016	DUC	SHPB	−3, −8, −18, −28	400–1000	–	Sand	–	1.6	10, 15, 30	–	–	ϕ30 × 18	T, $\dot{\varepsilon}$, ω
13	Ma et al., 2017	DUC	SHPB	−5, −15	160–265	0.5, 1, 1.5	Sandy clay	China (Shandong Province)	–	–	26.3	18.2	ϕ50 × 25	T, $\dot{\varepsilon}$, σ_3
14	Zhu et al., 2017	DUC	SHPB	−5, −15, −25	700–1200	–	Sand	–	1.6	30	–	–	ϕ30 × 18	T, $\dot{\varepsilon}$, particle size
15	Cao et al., 2018	DUC	SHPB	−5, −15, −25	500–950	–	–	–	1.6	30	–	–	ϕ30 × 18	T, $\dot{\varepsilon}$

(*continued on next page*)

Table 6 (*continued*)

No.	Refs.	Test conditions					Frozen soil samples							
		Type	Device	T (°C)	Loading (Default: $\dot{\varepsilon}$/s)	σ_3 (MPa)	Type	Location	ρ_{dry} (g/cm^3)	ω (%)	LL (%)	PL (%	Size (mm)	Influence factors
16	Zhang et al., 2018	Elastic wave test	Bending disks and bender elements	−10 to −2, 20	–	–	Clay, silt, and sand	North Slope of Alaska	1.6–2.07	–	24.4–33.4	15.4–24.4	ϕ75 × 100	T, soil type, depth
17	Fu et al., 2019a, b	DUC	SHPB	−5, −12, −19	500–1000	–	Sand	–	1.6	20	29.1	18.8	ϕ30 × 18	T, $\dot{\varepsilon}$
18	Fu et al., 2019c	DUC	SHPB	−5, −10, −15	300–900	–	Sand	–	1.6	15	29.1	18.8	ϕ30 × 18	T, $\dot{\varepsilon}$
19	Ma et al., 2019	DTC, DUC, and CSDL	Modified triaxial SHPB system	−10	285–407	0.819–4.641	Silty clay	China (Shanxi Province)	2.12	22.4	28.3	14.2	ϕ50 × 25	$\dot{\varepsilon}$, coupled static pre-stress and dynamic impact loading effect
20	Wang et al., 2019c	Small-strain loading test	S-wave velocity measurement apparatus	−10, −8, −6, −4, −2, 20	–	–	clay, silt and sand	Arctic Coastal Plane	1.601–2.108	16.6–37.8	24.4–33.4	15.4–24.4	ϕ70 × 140	Soil type, T
21	Zhu et al., 2019b	multiaxial loading (DUC and DUC with confining state)	Modified SHPB device with an aluminum sleeve offering passive confining pressure	−5, −12, −19	500–1100	–	Clay	China (Chengdu Province)	1.6	20	29.1	18.8	ϕ30 × 18	T, $\dot{\varepsilon}$
22	Zhang et al., 2019a	Cyclic DTC	Modified triaxial material test device (MTS-810)	−6	–	0.3–6	Silty soils with medium silica gravel	China (Gansu Province)	–	8.86	32.3	18.3	ϕ61.8 × 125	Different coarse-grained contents
23	Liu et al., 2020	Elastic wave test	Bender/extender elements	−20, 20	–	–	Sand-loess mixtures,	China (Loess Plateau)	–	–	–	–	ϕ50 × 100	Freeze-thaw cycles, sand content
24	Xu et al., 2020b	Cyclic DTC	–	−3, −5, −7, −9		0.2	Silty clay	China (Qinghai–Tibet Railway)	1.828	15	28	17.7	ϕ61.8 × 125	T, cyclic loading
25	Zhang et al., 2020b	DUC	Modified SHPB	−5, −15, −20	400–950	–	Clay	–	1.6	30	–	–	ϕ30 × 18	T, $\dot{\varepsilon}$
26	Zhao et al., 2020	Cyclic DTC	Triaxial material test device	−6	$\eta_\sigma = 0.7$ (1 HZ, sinusoidal loading form)	1, 3, 5, 8, 12, 14, 16, 18	Saline silty clay	China (Qinghai-Tibet plateau)	–	–	–	–	ϕ61.8 × 125	Initial static stress, loading cycle, and salt content (0, 0.5, 1.5, 2.5 %)
27	Zhu et al., 2020	DUC	Modified SHPB	−10, −15, −20	100–1200	–	Clay	China (Sichuna Province)	2.07	30	–	–	ϕ30 × 18	–
28	Fu et al., 2021	DUC	SHPB	−6, −10, −20, −30	100–700	–	Unsaturated sand	–	–	25	–	–	ϕ30 × 18	–
29	Ma et al., 2021a	DUC	SHPB	−10	120, 170, 220, 270	–	Silty soil	–	1.72	24.2	32.2	22.5	ϕ50 × 50	$\dot{\varepsilon}$, prefabricated crack number (0,1,2,3)
30	Ma et al., 2021b	DUC	SHPB				Clay			23.1	43	21	ϕ50 × 25	Pre-existing cracks with different

(*continued on next page*)

Table 6 (*continued*)

No.	Refs.	Test conditions					Frozen soil samples							
		Type	Device	T (°C)	Loading (Default: $\dot{\varepsilon}$/s)	σ_3 (MPa)	Type	Location	ρ_{dry} (g/cm^3)	ω (%)	LL (%)	PL (%	Size (mm)	Influence factors
														positions, numbers, lengths, and obliquities
31	Zhang et al., 2021	DUC	Modified SHPB	−10, −15, −20	200–1200		S Ling and	–	1.6	30	–	–	ϕ30 × 18	T, $\dot{\varepsilon}$
32	Zhang et al., 2021b		Frozen hollow cylinder apparatus (FHCA-300)	−8 to −15	Cyclic (0.2 Hz)	2.5	Clay	China (Qinghai-Tibet plateau)	1.77	19.8	27.7	17.6	ϕ60/ 100 (I/ O) × 200	T, cyclic stress ratio, principal stress rotation
33	Zhu et al., 2021a	DUC	SHPB	−5, −12, −19	500–1200	–	Sand	–	–	–	–	–	ϕ30 × 18	T, $\dot{\varepsilon}$
34	Zhu et al., 2021b	DUC	SHPB	−10, −15, −20	450–924	–	Clay		2.1	20			ϕ30 × 18	T, $\dot{\varepsilon}$
35	Li et al., 2022	DUC with F-T loading	SHPB	Freeze (−10, −15, −25) Thaw (5)	500	–	Sand	–	2	40	–	–	ϕ30 × 18	Number of F-T cycles (0, 1, 3, 5, 7)
36	Liu et al., 2022b	Elastic wave test	Bender elements	−20, 20	–	–	Loess	China (Lanzhou)	1.72	9.5, 13.5	–	17.7	ϕ50 × 100	Freeze-thaw cycles, salt content
37	Qiao et al. (2022)	DUC	SHPB	−10	300–800	–	Clay	–	–	20, 25, 30	–	–	ϕ30 × 18	$\dot{\varepsilon}$
38	Chunyu et al., 2023	DUC	SHPB	−10, −15, −20	308, 506, 686	–	Silty clay	–	–	–	–	–	ϕ30 × 18	T, $\dot{\varepsilon}$
39	Wang et al., 2023b	Cyclic DTC with F-T loading	Modified triaxial material test device (MTS-810)	Freeze (−10) Thaw (23)	η_σ = 0.8, 0.9, 0.98 (1 HZ, sinusoidal loading form)	0.3, 1, 1.4	Clay	China (Sichuan Province)	1.89	16.8	27.5	15.9	ϕ61.8 × 125	Number of F-T cycles (0, 1, 5, 20)
40	Zhang et al., 2022	Cyclic rotational shear tests	Frozen hollow cylinder apparatus (FHCA-300)	−10	Cyclic (0.1–2 Hz)	2.5	Clay	China (Qinghai-Tibet plateau)	1.77	19.8	27.7	17.6	ϕ60/ 100 (I/ O) × 200	Intermediate principal stress coefficient, rotation radius, frequency
41	Zhang et al., 2023a	DUC	SHPB	−10, −15, −20	350, 520, 820	–	Clay	–	–	30	–	–	ϕ30 × 18	Frozen soil with two different average sizes (1.7 and 0.725 mm) of coarse particles
42	Zhang et al., 2023b	DUC	SHPB	−5, −15, −25	350, 550, 750	–	Silty clay	China (Gansu Province)	1.6	20	–	–	ϕ30 × 18	–
43	Liu et al., 2024a, 2024b	Cyclic traffic loading test	Frozen hollow cylinder apparatus (FHCA)	−2	Cyclic (0.2 Hz)	0.1	Silt	China (Qinghai-Tibet plateau)	1.84	15	22.92	14.13	ϕ60/ 100 (I/ O) × 200	Principal stress direction, cardioid-shaped stress path,

(*continued on next page*)

Table 6 (*continued*)

No.	Refs.	Test conditions					Frozen soil samples							
		Type	Device	*T* (°C)	Loading (Default: $\dot{\varepsilon}$/s)	σ_3 (MPa)	Type	Location	ρ_{dry} (g/cm^3)	ω (%)	*LL* (%)	*PL* (%	Size (mm)	Influence factors
														energy dissipation.
44	Liu et al., 2025	Cyclic wave loading test	Hollow cylinder apparatus	−6	–	–	Silty Clay	China (Qinghai-Tibet plateau)	1.84	18.7	32.55	21.15	ϕ60/100 (I/O) × 200	Principal stress coefficient, mean principal stress, and principal stress rotation radius

Notes: DUC is dynamic uniaxial compression test (impact loading test); DTC is dynamic triaxial compression test; CSDL is coupled static and dynamic loading tests; LUC is loading-unloading cycles test; F-T is freeze-thaw loading; SHPB is split Hopkinson pressure bar (SHPB); modified SHPB refers to a variable cross-section bar is adopted as the incident bar; *T* is temperature; $\dot{\varepsilon}$ is strain rate; σ_3 is confining pressure; *f* is frequency; ρ_{dry} is dry density; ω is initial water content; *LL* and *PL* are liquid limit and plastic limit; η_σ is dynamic stress amplitude ratio, which equals the ratio of dynamic stress to the strength of frozen soil sample with corresponding confining pressure and salt content under static loading.

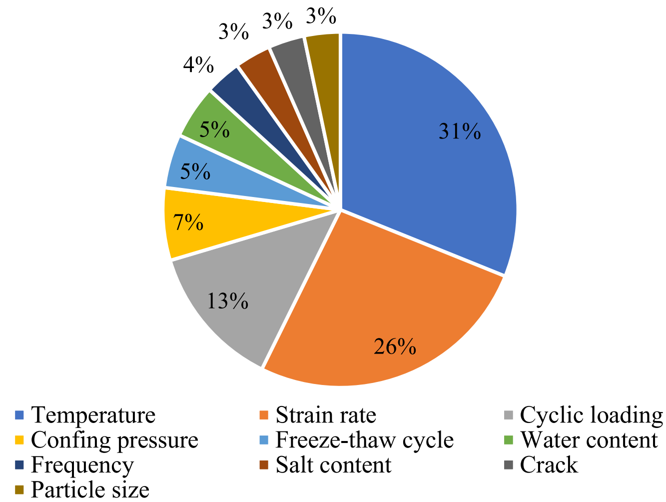

Fig. 7. Numbers of experimental studies on frozen soils with different influencing factors under dynamic loadings. Note: This figure is based on the studies reviewed in this work.

Additionally, Zhang et al. (2019a) conducted experiments using SHPB with an aluminum sleeve as a passive confining pressure device to examine the dynamic behaviors of frozen soils under multiaxial loading conditions. The results showed that the peak stress observed in the multiaxial state is significantly higher than in the uniaxial loading. Furthermore, unlike the failure model of frozen soil at a uniaxial state, the frozen soils under a passive confining pressure state displayed a viscoplastic failure mode.

Besides, some studies explored the effect of moisture content (Ling et al., 2009; Zhu et al., 2016), salt content (Zhao et al., 2020), particle size dependence (Zhu et al., 2017; Zhang et al., 2023a) and the effect of prefabricated cracks (Ma et al., 2021a) on the dynamic behaviors of frozen soils. The key dynamic behaviors of frozen soils under varying conditions are replotted in Fig. 9. It can be noted from Fig. 9(a) that the higher initial moisture content results in higher strength of frozen soils under impact loading states. Fig. 9(b) shows the relationship between accumulated shear strain and cyclic loading numbers for different Na_2SO_4 contents (i.e., 0 %, 0.5 %, 1.5 %, and 2.5 %) under $\sigma_3 = 5$ MPa in the work of Zhao et al. (2020). The results reveal that the salt content significantly influences the dynamic strength of saline soil. Notably, the dynamic strength of saline soil reaches its minimum and maximum values at $f_s = 0.5$ % and $f_s = 2.5$ %, respectively. When subjected to dynamic impact loading, the peak stresses of frozen soils are in the following order, from largest to smallest: fine particle specimens, mixed frozen soil specimens, middle particle specimens, and rough particle specimens (see Fig. 9(c)). Similar findings can be found in the impact loading tests conducted by Zhang et al. (2023a) on frozen soils with different average sizes (0.725 mm and 1.7 mm). Specifically, it was observed that the frozen soil mixed with 0.725 mm soil particles exhibited a higher strength compared to the mixture with 1.7 mm particles. Fig. 9(d) illustrates that prefabricated cracks contributed to a reduction in the dynamic compressive peak stress of the frozen silty soil specimen.

Dynamic properties (e.g., shear modulus, damping ratio, accumulative plastic strain) are important to evaluate the construction stability and safety. Compared to the experimental studies on the effect of cyclic loading on the static mechanical response of frozen soils, investigations on the dynamic behaviors of soils subjected to cyclic loading are relatively limited and still in the virgin stage of development, which needs to be further conducted. Vinson and his coauthors (e.g., Vinson, 1978; Vinson et al., 1978; Czajkowski and Vinson, 1980) are the pioneers in investigating the dynamic properties of frozen soil via cyclic loading. For example, Vinson (1978) summarized the dynamic properties of frozen

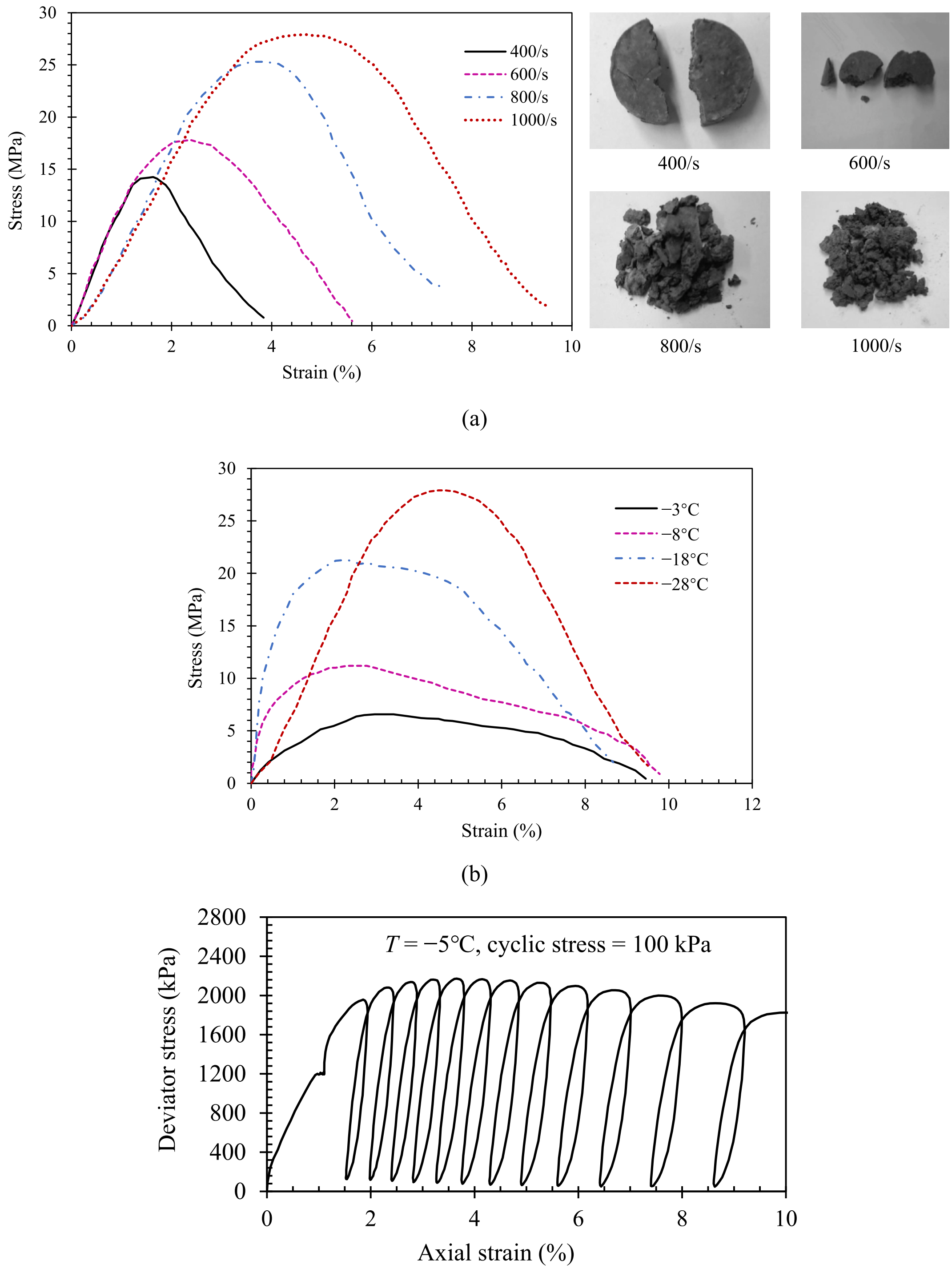

Fig. 8. Dynamic responses (a) stress-strain curves of frozen soil for different strain rates at $T = -18$ °C, $\omega = 15$ % and corresponding fracture modes of frozen soils after the SHPB tests (data from Zhu et al., 2016); (b) stress-strain curves of frozen soil for the different temperature at $\dot{\varepsilon} = 1000$/s, $\omega = 15$ % (data from Zhu et al., 2016); (c) stress-strain relationship of frozen silty clay under cyclic triaxial loading (data from Xu et al., 2020b).

soils from field and laboratory studies and indicated that the frozen soils' dynamic properties could be divided into two categories, including dynamic stress-strain properties (e.g., shear moduli, S wave velocity, longitudinal wave velocity) and energy absorbing properties (e.g., damping ratio, loss factor, attenuation coefficient). In recent years, Ling et al. (2013) conducted a series of cyclic triaxial tests on frozen soils and analyzed the influences of the dynamic axial stress amplitudes, confining stresses, temperatures, moisture contents, and salt contents on the stiffness and damping ratio under low-level repeated cyclic loading. Ling et al. (2015) investigated the influence of dynamic axial loading on frozen silty sand's dynamic features and fatigue. Zhang et al. (2019a) examined the impact of coarse-grained contents on the dynamic properties (i.e., stress-strain curves, hysteresis loops, accumulative plastic strain, dynamic strength, and damage variables, resilient modulus, damping ratios, accumulative plastic strain, dynamic strength, and damage variables) of frozen silty soils subjected to cyclic loadings. Zhao

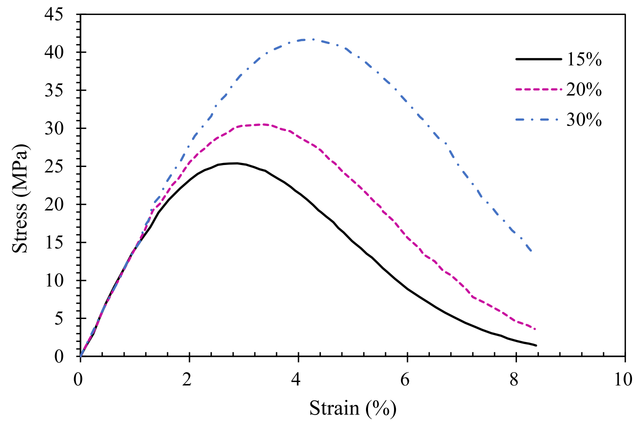

(a)

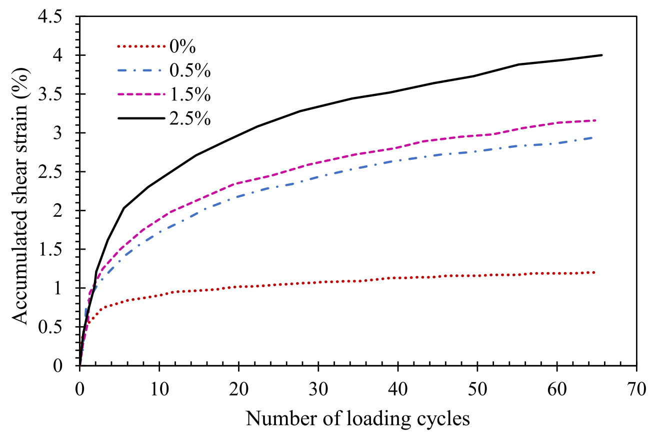

(b)

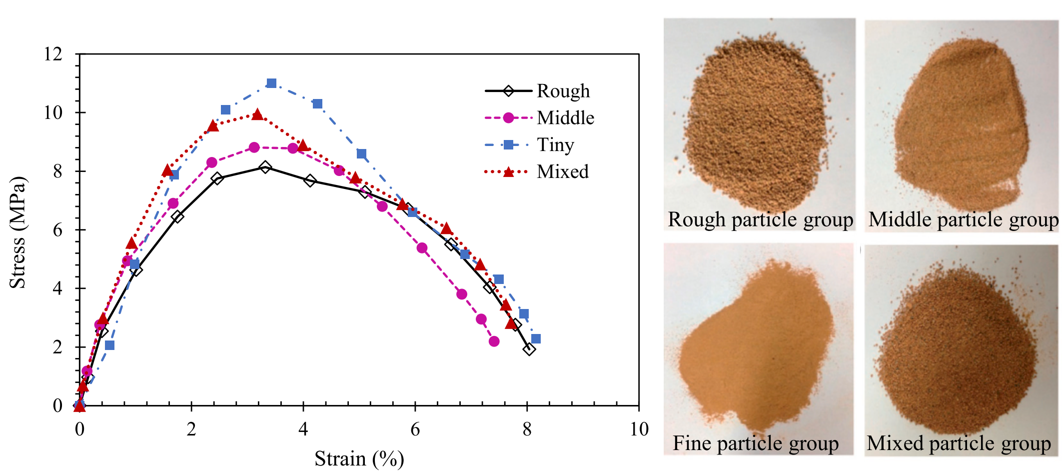

(c)

Fig. 9. Dynamic responses (a) stress-strain curves of frozen soils under different water content (data from Zhu et al., 2016); (b) accumulated shear strain and loading number of frozen saline soils with different salt contents (data from Zhao et al., 2020); (c) stress-strain curves of frozen soils with different particle sizes at $T = -5$ °C and $\dot{\varepsilon} = 900$/s (data from Zhu et al., 2017); (d) stress-strain curves of frozen soils with different crack numbers (data from Ma et al., 2021a).

et al. (2020) explored the dynamic behaviors of frozen saline soil under cyclic triaxial compression tests, and their results demonstrated that the salt contents and confining pressure could significantly affect the strength and deformation of frozen salty soils under cyclic loading. The tests of Zhang et al. (2019a) and Zhao et al. (2020) indicated that the stress-strain curves of frozen soils display strong nonlinearity, hysteresis, and strain accumulation.

Freeze-thaw cycles can also considerably affect frozen soils' dynamic mechanical behaviors. Ling et al. (2015) explored the dynamic shear modulus and damping ratio of frozen compacted sand subjected to

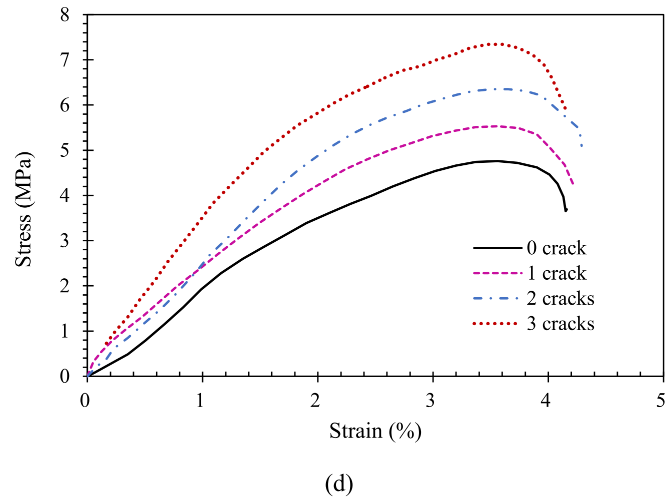

Fig. 9. (*continued*).

various freeze-thaw cycles, temperatures, initial moisture contents, loading frequencies, and confining pressures. Li et al. (2022) conducted experiments to explore the dynamic mechanical behaviors of frozen soils at varying numbers and temperatures of F-T cycles using the SHPB, where a gradual weakening of the peak stress as the number of F-T cycles increased until reaching the critical cycle number at which the soil specimen attains a steady state. Additionally, a decrease in the peak stress of the frozen soil with decreasing freezing temperatures could be noted in their measurement. Fig. 10 plots the variation on the frozen soil surface after several Freeze-Thaw cycles in Li et al. (2022), which depicts the micro-cracks on the sample surface increased with the number of F-T cycles. Considering the limited availability of references regarding the dynamic properties of frozen soil subjected to both freeze-thaw cycles and cyclic loading simultaneously, Wang et al. (2023) conducted dynamic cyclic triaxial experiments of frozen subgrade clay under cyclic loading conditions during freeze-thaw cycles. The experiments showed that the dynamic stress-strain and volumetric strain curves became progressively more dispersed and irregular after 20 F-T cycles. Additionally, the hysteresis loop curves, which represent the energy dissipation and deformation behavior during cyclic loading, exhibited a marked increase in loop area and deformation amplitude with increasing F-T cycles. Furthermore, as the number of freeze-thaw cycles increases, the axial accumulative strain, residual deformation, and damage variable of frozen clay also rise while the dynamic, resilient

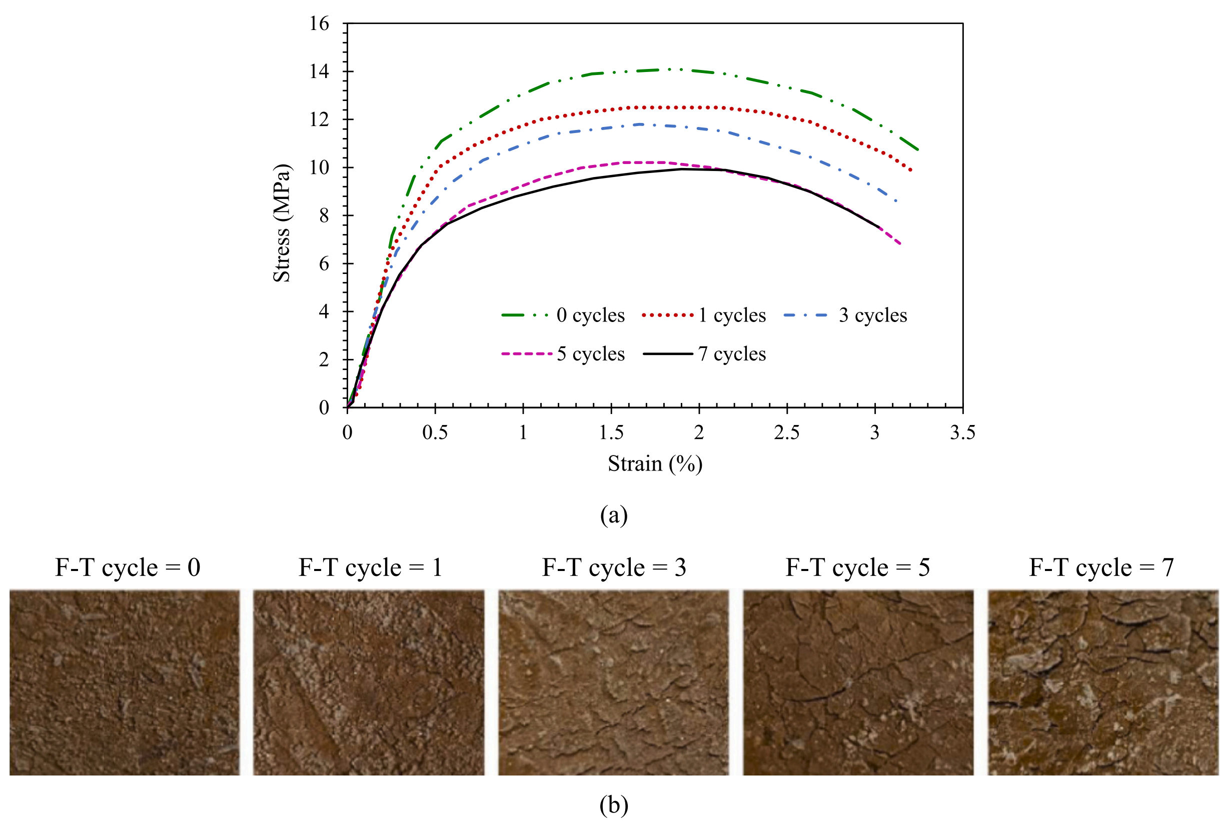

Fig. 10. Effect of Freeze-thaw cycles on dynamic behaviors of frozen soils (a) stress-strain curves under different numbers of F-T cycles at $T = -12$ °C; (b) variation of sample surfaces after F-T cycles (modified from Li et al. (2022)).

modulus and dynamic strength decrease.

4. Microscopic experiments on frozen soils

The microstructures of frozen soils alter during the freezing process due to the phase change and moisture migration, which not only affect the mechanical properties of frozen soils but also reflect the failure mechanism of frozen soils under external loadings (Ershov, 1988; Wang and Wang, 1998). At present, various advanced techniques have been utilized for microstructure characterizations, including scanning electron microscopy (SEM), computed tomography (CT), nuclear magnetic resonance (NMR), and mercury intrusion porosimetry (MIP). These

Table 7
Summary of typical investigations on microstructure variations of frozen soils.

Methods	Tests	Microstructure indexes	References	Influencing factors	Soil types
	Uniaxial creep test		Wu et al., 1995	T, σ_3 ($T = -5$ °C, stress = 3.5 MPa)	Loess soil
	Triaxial creep test	Crack	Ma et al., 1998	T, σ_3 ($T = -5$ °C, $\sigma_3 = 2$ MPa)	Loess soil
	Triaxial compression test		Zhang et al., 2019b	T, σ_3 ($T = -6$, -10 °C, $\sigma_3 = 0.5$, 1, 2, 3 MPa)	Silty clay-sand mixture
	F-T cycle test	Crack	Romanenko et al., 2017	F-T cycle ($NFT = 20$)	Loamy soils
		Pore and crack	Xu et al., 2021	F-T cycles, salinity ($NFT = 0$, 1, 2, 5, 10, $T_t = 20$ °C, $T_f = -20$ °C, salinity = 0.0 %, 0.5 %, 1.0 %, 1.5 %)	Saline intact loess
CT	Uniaxial compressive test	Damage	Qi et al., 2003	T, σ_3 ($T = -5$, -10 °C, $\sigma_3 = 0$, 1, 2, 3 MPa)	Loess soil
		Crack	Romanenko et al., 2017	F-T cycle ($NFT = 20$)	Loamy soils
		Pore and crack	Xu et al., 2021	F-T cycles ($NFT = 0$, 1, 2, 5, 10, $T_t = 20$ °C, $T_f = -20$ °C), salinity (0.0 %, 0.5 %, 1.0 %, 1.5 %)	Saline intact loess
	F-T cycle test		Chen et al., 2021	T, σ_3 ($T = -3$, -6, -10 °C, $\sigma_3 = 0.5$, 1, 2, 3 MPa)	Lanzhou loess
		CT value	Li et al., 2021a	T, σ_3 ($T = -2$, -5, -10, 15 °C, $\sigma_3 = 0.2$, 0.5, 1 MPa)	Graded gravel soil
			Sun et al., 2022	T, σ_3, ω ($T = -5$, -10, -15 °C, $\sigma_3 = 0$, 1, 3, 6, 8, 10, 12 MPa, ω (10.3 %, 16.6 %, 20.3 %)	Silty clay
	–	Ice lenses (Number, shape and thickness)	Wang and Wang, 1998	Soil type, salt, water, T, and overburden pressure (5)	Japanese volcanic ash, Linxia kaolinite, Inner Mongolia clay, Lanzhou silt, and Lanzhou sand
	Dynamic impact loading test, triaxial compressive tests	Particle (shape, arrangement, porosity, connectivity)	Hu et al., 2001	Numbers of repeated impact loads (1–8, 10, 13, 16, 20, 26, 32)	Loess
	Triaxial compression tests	Particle size and crack	Han et al., 2018	F-T cycles ($NFT = 0$, 1, 5, 10, 30, 60 and 120, $T_t = 20$ °C, $T_f = -20$ °C), salinity = 0, 0.5, 1, 2, 3 %, and $\sigma_3 = 0.1$, 0.2, 0.3 MPa	Saline clay
SEM		Particle size, crack and pores	Xu et al., 2018	F-T cycles ($NFT = 0$, 2, 5, 7, 10, 14, 17, 20)	Loess
		Pore number, porosity	Ding et al., 2019	F-T cycles ($NFT = 0$–2, $T_f = -10$, -20, -30 °C)	Marine clay
	F-T test	Proportion of pores and cracks	Wang et al., 2020a	F-T cycles ($NFT = 0$, 10, 60, 120, $T_t = 20$ °C, $T_f = -20$ °C), salinity (0, 0.5 %, 1 %, 2 %, 3 %)	Saline clay
		Particle size distribution, shape, arrangement, and intercontact	Zhao et al., 2023	F-T cycles ($NFT = 0$, 1, 3, 5, 10, 15, 20, 30, $T_t = 10$ °C, $T_f = -10$ °C, $\sigma_3 = 0.05$, 0.1, 0.2 MPa)	Loess
	Dynamic triaxial instrument	Particle distribution and porosity	Jiang et al., 2023	T, σ_3 ($T = 0$, -2, -5, -10, -15 °C, $\sigma_3 = 0.15$ MPa)	Silt clay
NMR	Uniaxial compression test	^{1}H signal intensity	Ren et al., 2023b	ω ($\omega = 17$ %, 20 %, 23 %, $T_f = -10 \sim -180$ °C)	Clay
SEM, LDA	Triaxial compression test ($T = -6$ °C, $\sigma_3 = 2$ MPa)	Particle size	Zhang et al., 2019c	F-T cycles ($NFT = 1$, 3, 5, 9, 15, 20, 30, 50, $T_t = 25$ °C, $T_f = -15$ °C)	Silty sand
	Triaxial compression test ($T = -6$ °C, $\sigma_3 = 2$ MPa)	Pores	You et al., 2017	Salinity (0, 0.5 %, 1.5 %, 2.5 %)	Silty clay
SEM, MIP	Unidirectional freezing tests	Pores (Porosity, volume)	Zhang et al., 2023c	$\omega = 10$ %, 14 %, 18 %, $T_f = -5$, -10 °C	Silt
	Dynamic triaxial test	Pores (number, size, shape, distribution, arrangement, volume, contact type, and cementation type)	Wen et al., 2023	Temperature rise gradient ($T = 0$, -5, -10, -15, -20 °C,	Silty clay
	Uniaxial compressive test	Unfrozen water content, particle size and crack	Ma et al., 1999	T, stress ($T = -5$ °C, stress = 0, 8, 10, 16 MPa)	Lanzhou fine sand and Huaibei silty clay
SEM, NMR		Pore ratio and size	Li et al., 2021b	F-T cycles ($NFT = 0$, 1, 2, 4, 6, 10, $T_t = 25$ °C, $T_f = -20$ °C)	Expensive soils
	Freezing test	Pore size and ratio, damage	Kong et al., 2022	Freezing duration = 1, 2, 4, 6, 12, 18, 24 h, pressure = 0.05, 0.1, 0.2, 0.4 MPa, $T_f = -3$, -8, -20 °C	Soft clay

Notes: T is temperature; T_t is thaw temperature; T_f is freezing temperature; ω is water content; σ_3 is confining pressure; scanning electron microscopy (SEM), computed tomography (CT), nuclear magnetic resonance (NMR), mercury intrusion porosimetry (MIP); Laser diffraction analysis (LDA); F-T is freeze-thaw; NFT is the number of freeze-thaw cycles.

methods provide critical insights into crack propagation, pore evolution, particle arrangement, and moisture distribution, which are essential for understanding the behavior of frozen soils under different environmental and mechanical conditions.

4.1. Computed tomography (CT) analysis

Computer tomography (CT) offers a promising method to dynamically monitor structural variation within frozen soils (Wu and Ma, 1994). The CT technique employs X-rays to penetrate the object slice and measure the attenuation of X-rays, which allows for the assessment of density variations within the sample. The CT value, which reflects the average density distribution of particles, ice, and unfrozen water, is commonly used to characterize microstructural changes. A higher CT value indicates a denser material, and variations in CT values can be used to track changes in soil structure during loading or freeze-thaw cycles (Qi et al., 2003).

As shown in Table 7, CT analysis has been widely applied to investigate crack formation, pore distribution, and density variations in frozen soils. Studies have shown that under creep conditions, microdefects redistribute in the stable creep stage, with smaller cracks closing and larger cracks propagating and interconnecting to form microfractures. As stress increases, an accelerated creep stage occurs, leading to complete failure (Wu et al., 1995; Ma et al., 1998). Additionally, triaxial tests have revealed that confining pressure plays a crucial role in crack development, where higher confining pressures suppress crack growth initially but may lead to pressure melting of ice at excessive levels, resulting in water migration and microcrack formation (Qi et al., 2003; Chen et al., 2021; Li et al., 2021a). F-T cycles are another key factor influencing frozen soil microstructures. Studies using CT imaging have demonstrated that F-T cycles cause the progressive expansion of small pores and the formation of cracks, which are particularly pronounced in saline soils where salt crystallization amplifies structural degradation (Romanenko et al., 2017; Xu et al., 2021). The interplay between salinity and freeze-thaw effects has been observed in graded gravel soils as well, where confining pressure induces partial melting of pore ice, leading to pore expansion and microcrack development (Sun et al., 2022).

4.2. Scanning electron microscopy (SEM) analysis

The SEM technique has been widely employed to observe the microstructure evolution of frozen soils that were once frozen under complex loadings (see Table 7). While SEM offers high-resolution imaging of soil microstructures, it is important to note that common SEM techniques operate under high-vacuum conditions, which result in the sublimation of ice within frozen soils (Chen et al., 2024). Therefore, the SEM images presented in this study do not capture the intact ice structure of frozen soils but instead reveal the residual microstructural features of soils that are once frozen, such as pore morphology, particle arrangement, and crack propagation. Despite this limitation, SEM studies have provided valuable insights into the effects of freeze-thaw cycles, salinity, and mechanical loading on frozen soil microstructure. For instance, repeated impact loading has been shown to increase aggregate size while modifying particle orientation and connectivity (Hu et al., 2001). Triaxial compression tests reveal that F-T cycles lead to significant changes in particle size and crack development, with the effects of freeze-thaw being more pronounced than those of salinity alone (Han et al., 2018). Additionally, freeze-thaw cycles fragment larger soil aggregates, promoting the formation of fine pores and increasing overall porosity (Xu et al., 2018).

Fig. 11 shows the SEM images of saline silty sand under different F-T cycles conducted by Zhang et al. (2019c). It can be noted from Fig. 11(a-1) and Fig. 11(b-1) that the salt-free frozen soils remain structurally stable after 3 F-T cycles, with tight particle arrangement and small pores. However, after nine cycles, frost heave disrupts the structure, which causes increasing porosity and reduced particle size (see Fig. 11(c-1)). As fine particles fill pores, the porosity gradually decreases (see Fig. 11(d-1) and Fig. 11(e-1)). In contrast, frozen soil with 2 % salt content maintains its structure initially, as shown in Figs. 11(a-2) and 11(b-2). As F-T cycles progress, moisture causes volume expansion, destroying the soil structure due to salt crystallization. After 20 cycles, the soil becomes loose with larger pores (Fig. 11(d-2)). Frequent F-T cycles and salt expansion break down particles, increasing fine particles and reducing porosity, while smaller particles decrease frost heaving and salt expansion, ultimately reaching a new structural equilibrium (Fig. 12(e-2)).

4.3. Pore structure and moisture distribution analysis

To complement SEM observations, mercury intrusion porosimetry (MIP) and nuclear magnetic resonance (NMR) have been employed to quantify pore size distribution and analyze moisture dynamics in frozen soils. MIP studies have demonstrated that freeze-thaw cycles significantly increase pore volume and alter pore connectivity, with saline soils showing a higher proportion of fine pores after multiple freeze-thaw cycles (Wang et al., 2020a). NMR analysis has further revealed that higher initial water content leads to greater unfrozen water content, which weakens soil strength and promotes deformation (Ren et al., 2023b).

Moreover, research has shown that salinity influences pore evolution in complex ways. At low concentrations, salt dissolution increases the volume of unfrozen water, enhancing porosity. However, at higher concentrations, salt crystallization fills the pores, reducing porosity and reinforcing soil strength through interlocking effects (You et al., 2017). Temperature gradients also play a crucial role, with lower temperatures leading to a more compact and uniform soil structure, while higher temperatures increase pore connectivity and overall porosity (Wen et al., 2023).

As illustrated in Fig. 12, influencing factors such as temperature, confining pressure, freeze-thaw cycles, and salinity have been extensively studied, with temperature and F-T cycles each accounting for 23 % of reviewed studies. Overall, microscopic tests on frozen soils are efficient tools to analyze the microstructure variation of frozen soils with the advantages of high magnifications and resolutions, which provide detailed information for understanding the mechanical behaviors of frozen soils and enable better engineering practices, infrastructure design, and environmental management in cold regions.

5. Discussion

5.1. Advancement in experimental tests

The aforementioned studies represent experimental investigations into the mechanical behaviors of frozen soils under static and dynamic loads. Currently, most static tests on frozen soils have focused on simple loadings, such as uniaxial compression, triaxial compression, tensile, and direct shear tests. Dynamic tests on frozen soils are typically conducted employing specialized devices such as the split Hopkinson pressure bar (SHPB). A range of environmental factors (e.g., temperature, strain rate, confining pressure, freeze-thaw cycles, frequency) and soil properties (e.g., water content, salt content, crack, and particle size) that can influence the mechanical behaviors of frozen soils have been discussed. However, the majority of experiments have focused solely on examining the influences of individual, two, or three factors, and the coupled effect of these factors on the dynamic behaviors of frozen soils remains unclear.

Significant advancements have been made in recent years to address the limitations of traditional testing methodologies for frozen soils, which aim to improve the accuracy and reliability of experimental results and provide deeper insights into the fundamental mechanisms governing the behavior of frozen soils. Herein, some typical

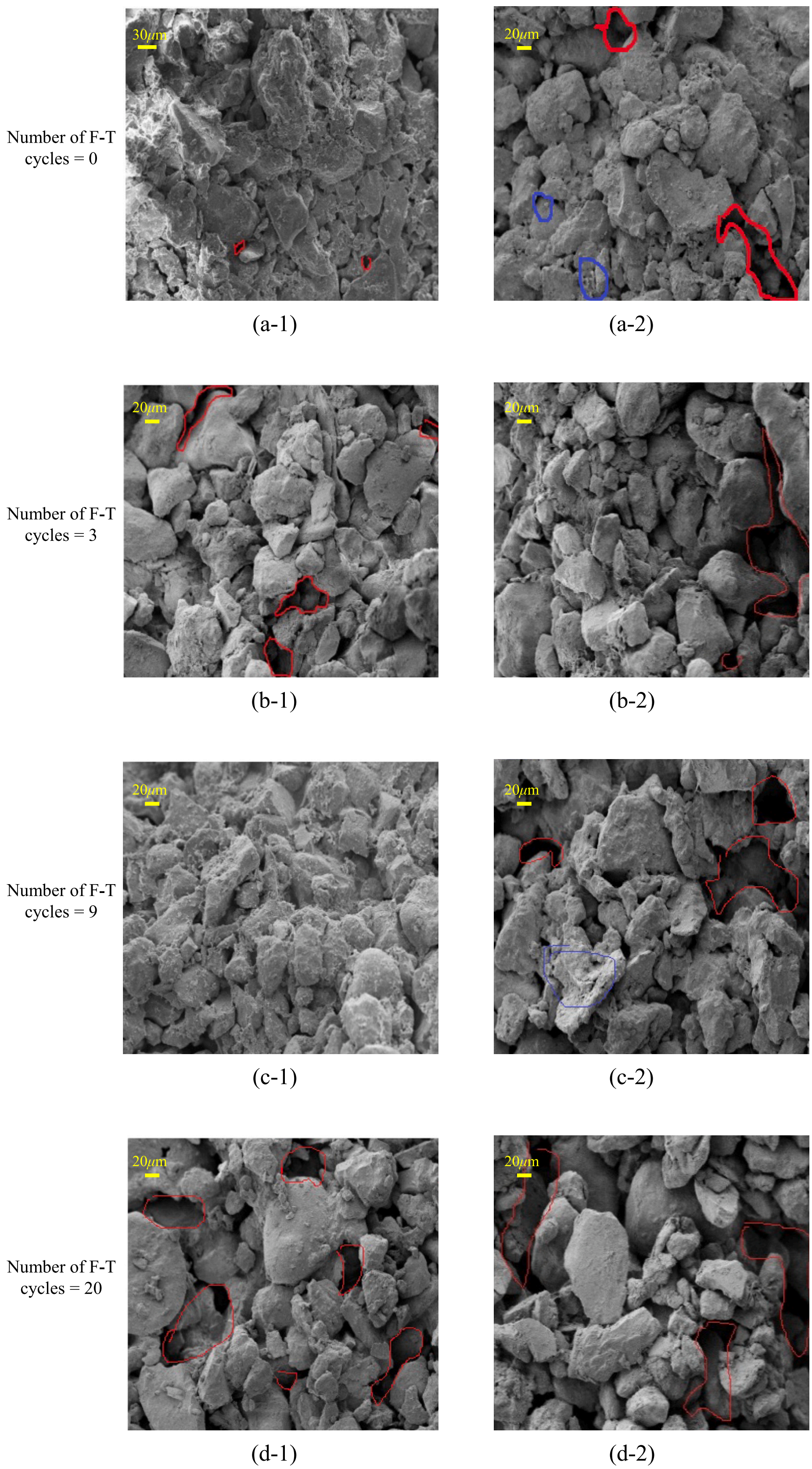

Fig. 11. SEM images of saline frozen soil (1) salt content =0 %; (2) salt content = 2 %; (a) 0 freeze-thaw cycles; (b) 3 freeze-thaw cycles; (c) 9 freeze-thaw cycles; (d) 20 freeze-thaw cycles; (e) 50 freeze-thaw cycles. Figures are modified from Zhang et al. (2019c).

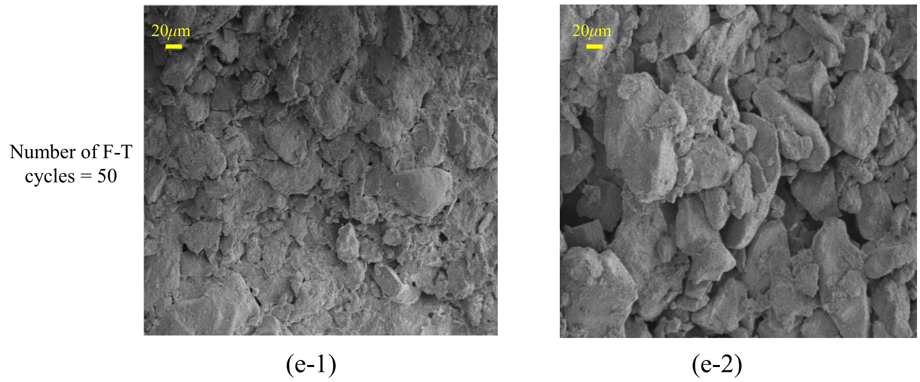

Fig. 11. (*continued*).

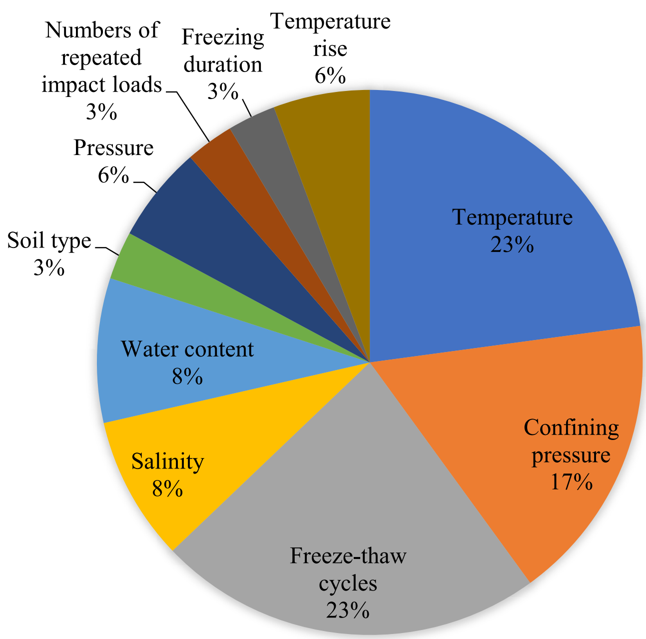

Fig. 12. Proportion of influencing factors in existing microscopic tests on frozen soils.

advancements in testing are summarized as follows.

(1) True triaxial testing systems

Traditional triaxial compression tests, widely used in frozen soil research, are limited in their ability to simulate the true stress states encountered in engineering applications. To address these limitations, true triaxial testing systems have been developed (e.g., Huang et al., 2022). This system enables a more accurate representation of field stress conditions, providing insights into the anisotropic mechanical behavior of frozen soils, which is often neglected in classical studies.

(2) Temperature-controlled testing systems with pore pressure measurement

Pore pressure and suction measurements are central to unfrozen soil mechanics, especially in unsaturated soils. For example, the application of pore pressure transducers in frozen soil research represents a significant step toward understanding coupled THM behavior in frozen soils. For example, Lyu et al. (2021a,b) proposed a system capable of maintaining precise thermal conditions while simultaneously measuring under isotropic and deviatoric loading. This system employs antifreeze-saturated porous stones and high-precision transducers, ensuring hydraulic connectivity at subzero temperatures and enabling accurate monitoring of pore pressure evolution during freezing and thawing processes. The measurement of PWP provides critical insights into the effects of confining pressure and strain rate, bridging the gap between empirical observations and theoretical models.

(3) High-precision instrumentation for small-strain behavior

The small-strain deformation characteristics of frozen soils have received increased attention due to their critical importance in understanding stiffness, stress-strain relationships, and the onset of yielding. High-precision instrumentation, such as bender elements and local displacement transducers, has enabled accurate measurements of stiffness and strain at resolutions as small as 0.001 %. For example, Nishimura et al. (2019) conducted a comparative study on the small-strain deformation behavior of frozen and unfrozen Kasaoka clay. By employing a temperature-controlled triaxial apparatus with semi-local instrumentation for axial strain and a newly designed miniature freezing cell for dynamic testing, the study demonstrated that frozen clay exhibits stiffness behavior qualitatively similar to unfrozen clay at strains below 0.002 %. Such findings highlight the importance of high-precision systems in capturing subtle, state-dependent behaviors. In parallel, unfrozen soil mechanics have long utilized similar instrumentation, such as bender elements, to investigate small-strain stiffness and shear wave velocity.

(4) Hollow cylinder apparatus

The adoption of hollow cylinder apparatus (HCA) represents another breakthrough in frozen soil testing. For example, Zhao et al. (2019) utilized the frozen hollow cylinder apparatus (FHCA) to investigate the deformation behavior of frozen soils under radial thermal gradients. Some scholars have employed the FHCA to explore the effects of principal stress direction on the anisotropic behavior and capture the mechanical behaviors of frozen soils under stress conditions closer to real-world scenarios, such as wave loads and traffic-induced stresses (Chen et al., 2022; Liu et al., 2024a, 2024b; Liu et al., 2025). In unfrozen soil mechanics, HCAs have been extensively used to explore anisotropy, small-strain stiffness, and rotational shear behavior. The delayed application of this apparatus in frozen soil research highlights the need for further efforts to bridge the methodological gap between the two fields.

It can be concluded that the testing methodologies in frozen soil mechanics have historically lagged behind those in unfrozen soil mechanics, where techniques such as bender elements, hollow cylinder apparatus, and true triaxial tests have been widely adopted for decades. However, recent advancements in frozen soil testing are closing this gap. These advancements not only enhance our understanding of frozen soil mechanics but also provide valuable insights for infrastructure design and maintenance in cold regions.

5.2. *Advancement in microstructural observations*

Regarding the microstructural investigations on frozen soils, numerous studies reported the microstructure changes in frozen soils under complex conditions (e.g., F-T cycles) or possessing different properties (e.g., salinity). The widely used techniques are SEM and CT, which enable the quantitative determination of micropore morphology (e.g., pore size, shape, distribution, arrangement, contact type, and cementation type) and particle features (e.g., size, ratio, volume) of frozen soil. To address the limitations of individual methods, researchers have combined multiple techniques to comprehensively investigate microstructural variations in frozen soils. For instance, SEM tests are prone to human interpretation errors and are limited in their ability to assess a broad range of pore sizes, whereas MIP tests may introduce inaccuracies due to the presence of irregular'gourd-shaped' pores. Accordingly, coupling SEM and MIP tests is an efficient approach to accurately capturing the micro characteristics of frozen soil. However, some limitations of existing microstructural techniques should be addressed.

(1) The standardization of sample preparation and testing operation is still lacking. Unified protocols for preparing and testing frozen soil samples are essential to minimize artifacts and ensure consistency across studies. The preparation and testing of frozen soils can involve artifacts and modify the original microstructure of frozen soils. Different studies may employ various techniques, sample preparation methods, and analysis approaches, making it challenging to compare and integrate findings across various investigations.

(2) Microscopic tests are typically conducted on small-scale samples, which may not fully represent the heterogeneity of natural frozen soil conditions. Future work should explore scaling-up microstructural studies to account for the inherent variability in frozen soils. Besides, some microscopic techniques, e.g., SEM, could only provide two-dimensional (2D) observations and cannot fully capture the three-dimensional structure of the entire frozen soil specimen. Integrating SEM with 3D imaging techniques, such as X-ray micro-CT, could provide richer datasets to improve our understanding of frozen soil structure.

(3) Current technologies fail to capture the time-dependent behaviors and variations in microstructures of in-situ frozen soils. The behaviors of frozen soils are time-dependent, while the microstructural techniques provide snapshots of the microstructure of frozen soils at a small scale and at a specific moment. Moreover, conducting microscopic tests directly in the field or in situ frozen soil conditions remains technically challenging. Developing portable devices for in-situ microstructural analysis or improving laboratory-based simulations of field conditions could address this limitation.

5.3. Extensions to frozen soil analogs

Apart from traditional frozen soil, some special soils display characteristics similar to those of frozen soils, e.g., methane hydrates sediments and water ice-bearing lunar regolith. Recent findings indicate that methane hydrates sediments might coexist with ice (Yakushev and Chuvilin, 2000; Li et al., 2016; Yang et al., 2019), and their mechanical properties are similar to those of frozen soils owing to their similarity in temperature and morphology (Li et al., 2011b; Miyazaki et al., 2011; Chen et al., 2023). However, despite extensive investigations on frozen soils' mechanical and rheological properties, limited studies have been conducted on methane hydrate sediments, leading to a lack of fundamental understanding regarding their unique characteristics. The development of experimental methods to simulate the combined effects of gas hydrate dissociation and freezing processes is essential for understanding their mechanical stability. In addition, investigations have been conducted to explore the geotechnical properties of lunar regolith simulants containing ice, employing various laboratory techniques, including unconfined compression tests, cone penetration tests, and Brazilian tensile strength tests (Gertsch et al., 2008; Pitcher et al., 2016; Wardak, 2021). By freezing a mixture of liquid water and dry regolith simulant, researchers have created "mud-pies" that closely resemble the physical textures of terrestrial frozen soils and analyzed the relationships of icy lunar regolith strength and other factors such as ice content, temperature, density, vacuum pressures, and volatile composition (Ricardo et al., 2023). Numerous studies have highlighted the significant influence of ice morphology on the mechanical behaviors of icy lunar regolith, but few investigations have comprehensively explored their relationships. Future research in this area should focus on quantifying the effects of ice morphology, developing constitutive models for extraterrestrial applications, and creating standardized testing protocols for icy regolith simulants. Hence, existing experiments on frozen soils are helpful for elucidating the mechanical responses of these geomaterials that resemble frozen soils and offer potential avenues for further research directions.

6. Conclusions and future works

This current review depicts a comprehensive summary of the up-to-date experiments on the mechanical behaviors of frozen soils, which discuss the advanced test devices and shed light on the macro and micro responses of frozen soils under complex conditions. The primary conclusions are drawn as follows.

(1) Experiment aspect:

Over the last few decades, extensive experimental investigations have been conducted to explore the mechanical behaviors of frozen soils under static and dynamic loadings. Despite significant advancements, several gaps remain in the understanding of frozen soil mechanics under realistic and complex stress conditions. Traditional experimental studies often focus on uniaxial or triaxial conditions, and few of them address the impact of intermediate principal stress and complex stress paths. Furthermore, while the roles of some factors, such as temperature and confining pressure, are well-documented, the coupled effects of multiple influencing factors remain unclear. Recent developments in experimental tests using advanced equipment such as SHPB, frozen hollow cylinder apparatus, and microstructural investigation methods (e.g., CT scanning, NMR) provide opportunities to address these gaps. The anisotropic effects, small-strain stiffness, and stochastic distribution of ice lenses deserve further exploration, especially under freeze-thaw cycles and dynamic loading.

In addition, existing experimental tests under static or dynamic loadings are primarily conducted in the laboratory, and measured data from in-situ soil samples is still lacking. Under complex loading conditions and climate change, long-term field monitoring data on frozen soils are also imperative.

(2) Microstructural observation aspects:

It is essential to acknowledge the challenges in sample representativeness, imaging depth, and standardized sample preparation and testing when interpreting the microscopic observations on frozen soils. Additionally, integrating multiple techniques and considering long-term effects and in-situ observations are essential for a more comprehensive understanding of the microstructural characteristics and behaviors of frozen soils.

(3) Available database aspect:

An open database of experimental data on frozen soils is vital for validating constitutive models and beneficial for the models' reliability and generalizability. Hence, to facilitate the constitutive model validation process and promote further research and practical applications, it would be helpful to establish a comprehensive database that consolidates information on the mechanical behaviors of frozen soils. This database can be constructed by incorporating data from scientific publications and government reports, providing a valuable resource for the constitutive modeling of frozen soils and references for understanding the multi-physics interactions within frozen soils (Li et al., 2024a; Li and Yin, 2024).

CRediT authorship contribution statement

Kai-Qi Li: Writing – review & editing, Writing – original draft, Validation, Software, Methodology, Investigation, Formal analysis, Data curation, Conceptualization. **Zhen-Yu Yin:** Writing – review & editing, Writing – original draft, Supervision, Funding acquisition. **Zhao-Hui Yang:** Writing – review & editing, Writing – original draft, Validation, Data curation. **Yong Liu:** Writing – review & editing, Writing – original draft, Formal analysis.

Declaration of competing interest

The authors declare that they have no known competing financial interests or personal relationships that could have appeared to influence the work reported in this paper.

Acknowledgements

This research was financially supported by the Research Grants Council (RGC) of Hong Kong Special Administrative Region Government (HKSARG) of China (General Research Fund, Grant No. 15226322, 15227624) and the National Natural Science Foundation of China (Grant No. U22A20596).

Data availability

All data that support the findings of this study are available from the corresponding author upon reasonable request.

References

Alkire, B.D., Andersland, O.B., 1973. The effect of confining pressure on the mechanical properties of sand–ice materials. J. Glaciol. 12 (66), 469–481.
Andersland, O.B., Ladanyi, B., 2003. Frozen ground engineering. John Wiley & Sons.
Azmatch, T.F., Sego, D.C., Arenson, L.U., Biggar, K.W., 2011. Tensile strength and stress–strain behavior of Devon silt under frozen fringe conditions. Cold Reg. Sci. Technol. 68 (1–2), 85–90.
Bray, M.T., 2012. The influence of cryostructure on the creep behavior of ice-rich permafrost. Cold Reg. Sci. Technol. 79, 43–52.
Cao, C., Zhu, Z., Fu, T., Liu, Z., 2018. A constitutive model for frozen soil based on rate-dependent damage evolution. Int. J. Damage Mechan. 27 (10), 1589–1600.
Chamberlain, E., Groves, C., Perham, R., 1972. The mechanical behavior of frozen earth materials under high pressure triaxial test conditions. Géotechnique 22 (3), 469–483.
Chang, D., Lai, Y., Yu, F., 2019. An elastoplastic constitutive model for frozen saline coarse sandy soil undergoing particle breakage. Acta Geotech. 14 (6), 1757–1783.
Chang, D., Yan, Y., Liu, J., Xu, A., Feng, L., Zhang, M., 2023. Micro-macroscopic mechanical behavior of frozen sand based on a large-scale direct shear test. Comput. Geotech. 159, 105484.
Chen, D., Wang, D., Ma, W., Lei, L., Li, G., 2019. A strength criterion for frozen clay considering the influence of stress Lode angle. Can. Geotech. J. 56 (11), 1557–1572.
Chen, S., Ma, W., Li, G., 2021. A novel approach for characterizing frozen soil damage based on mesostructure. Int. J. Damage Mechan. 31 (3), 444–463.
Chen, D., Li, G., Zhao, X., et al., 2022. Experimental study on the anisotropy and non-coaxiality of frozen standard sand under different principal stress directions. Geofluids 2022 (1), 1585324.
Chen, M., Li, Y., Zhang, Y., Qi, M., Wu, N., 2023. Recent advances in creep behaviors characterization for hydrate-bearing sediment. Renew. Sust. Energ. Rev. 183, 113434.
Chen, Q., Ghimire, B., Su, L., Liu, Y., 2024. Micro-scale investigations on the mechanical properties of expansive soil subjected to freeze-thaw cycles. Cold Reg. Sci. Technol. 219, 104128.
Christ, M., Kim, Y.C., Park, J.B., 2009. The influence of temperature and cycles on acoustic and mechanical properties of frozen soils. KSCE J. Civ. Eng. 13, 153–159.
Chunyu, Z., Zhu, Z., Li, B., Li, T., 2023. Numerical simulation research on impact mechanical properties of frozen soil based on discrete element method. Int. J. Damage Mechan. 32 (3), 442–461.
Classen, J., Hoppe, P., Seegers, J., 2019. Ground freezing and excavation of the museum island metro station under a river in central berlin–challenges and experiences. In: Tunnels and Underground Cities. Engineering and Innovation Meet Archaeology, Architecture and Art. CRC Press, pp. 1314–1322.
Cui, Z.D., He, P.P., Yang, W.H., 2014. Mechanical properties of a silty clay subjected to freezing–thawing. Cold Reg. Sci. Technol. 98, 26–34.
Czajkowski, R.L., Vinson, T.S., 1980. Dynamic properties of frozen silt under cyclic loading. J. Geotech. Eng. Div. 106 (9), 963–980.
Ding, Z., Kong, B., Wei, X., Zhang, M., Xu, B., Zhao, F., 2019. Laboratory testing to research the micro-structure and dynamic characteristics of frozen–thawed marine soft soil. J. Marine Sci. Eng. 7 (4), 85.
Ershov, E.D., 1988. Microstructure of Frozen Soil. Moscow University Press (in Russian).
Esmaeili-Falak, M., Katebi, H., Javadi, A., 2018. Experimental study of the mechanical behavior of frozen soils-a case study of Tabriz subway. Periodi. Polytech. Civil Eng. 62 (1), 117–125.
Fei, W., Yang, Z.J., 2019. Modeling unconfined compression behavior of frozen Fairbanks silt considering effects of temperature, strain rate and dry density. Cold Reg. Sci. Technol. 158, 252–263.
Fish, A.M., Zaretsky, Y.K., 1997. Ice Strength as a Function of Hydrostatic Pressure and Temperature.
Fu, T., Zhu, Z., Cao, C., 2019a. Constitutive model of frozen-soil dynamic characteristics under impact loading. Acta Mech. 230 (5), 1869–1889.
Fu, T., Zhu, Z., Cao, C., 2019b. Simulating the dynamic behavior and energy consumption characteristics of frozen sandy soil under impact loading. Cold Reg. Sci. Technol. 166, 102821.
Fu, T., Zhu, Z., Zhang, D., Liu, Z., Xie, Q., 2019c. Research on damage viscoelastic dynamic constitutive model of frozen soil. Cold Reg. Sci. Technol. 160, 209–221.
Fu, T., Zhu, Z., Ma, W., Zhang, F., 2021. Damage model of unsaturated frozen soil while considering the influence of temperature rise under impact loading. Mech. Mater. 163, 104073.
Furnish, M.D., 1998. Measuring static and dynamic properties of frozen silty soils. (no. SAND98-1497). Sandia National Lab.(SNL-NM), Albuquerque, NM (United States); Sandia National Lab.(SNL-CA), Livermore, CA (United States).
Gagnon, R.E., Gammon, P.H., 1995. Triaxial experiments on iceberg and glacier ice. J. Glaciol. 41 (139), 528–540.
Gertsch, L.S., Rostami, J., Gustafson, R., 2008. Review of lunar regolith properties for design of low power lunar excavators. In: 6 Th International Conference on Case Histories in Geotechnical Engineering, p. 10.02.
Girgis, N., Li, B., Akhtar, S., Courcelles, B., 2020. Experimental study of rate-dependent uniaxial compressive behaviors of two artificial frozen sandy clay soils. Cold Reg. Sci. Technol. 180, 103166.
Han, Y., Wang, Q., Wang, N., Wang, J., Zhang, X., Cheng, S., Kong, Y., 2018. Effect of freeze-thaw cycles on shear strength of saline soil. Cold Reg. Sci. Technol. 154, 42–53.
He, Y.Q., Liao, H.J., Wu, W., Wang, S., 2023. Hypoplastic modeling of inherent anisotropy in normally and overconsolidated clays. Acta Geotech. 18 (12), 6315–6333.
He, J., Niu, F., Jiang, H., Jiao, C., 2023a. Fractional viscoelastic-plastic constitutive model for frozen soil based on microcosmic damage mechanism. Mech. Mater. 177, 104545.
He, J., Niu, F., Su, W., Jiang, H., 2023b. Nonlinear unified strength criterion for frozen soil based on homogenization theory. Mech. Adv. Mater. Struct. 30 (19), 4002–4015.
Hivon, E.G., Sego, D.C., 1995. Strength of frozen saline soils. Can. Geotech. J. 32 (2), 336–354.
Hou, F., Lai, Y., Liu, E., Luo, H., Liu, X., 2018. A creep constitutive model for frozen soils with different contents of coarse grains. Cold Reg. Sci. Technol. 145, 119–126.
Hu, R.L., Yeung, M.R., Lee, C.F., Wang, S.J., 2001. Mechanical behavior and microstructural variation of loess under dynamic compaction. Eng. Geol. 59 (3–4), 203–217.
Huang, K., Ma, Q., Ma, D., Yao, Z., 2022. Strength and deformation properties of frozen sand under a true triaxial stress condition. Soils Found. 62 (1), 101089.
Jiang, N., Li, H., Liu, Y., Li, H., Wen, D., 2023. Pore microstructure and mechanical behavior of frozen soils subjected to variable temperature. Cold Reg. Sci. Technol. 206, 103740.
Johnson, T.C., Cole, D.M., Chamberlain, E.J., 1979. Effect of freeze-thaw cycles on resilient properties of fine-grained soils. Eng. Geol. 13 (1–4), 247–276.
Jones, S.J., 1982. The confined compressive strength of polycrystalline ice. J. Glaciol. 28 (98), 171–178.
Kolsky, H., 1949. An investigation of the mechanical properties of materials at very high rates of loading. Proceed. Phys. Soc. Sect. B 62 (11), 676.
Kong, B., He, S.H., Tao, Y., Xia, J., 2022. Pore structure and fractal characteristics of frozen–thawed soft soil. Fract. Fract. 6 (4), 183.
Kotov, P.I., Stanilovskaya, J.Y.V., 2021. Predicting changes in the mechanical properties of frozen saline soils. Eur. J. Environ. Civ. Eng. 26 (12), 5716–5772.
Ladanyi, B., 1972. An engineering theory of creep of frozen soils. Can. Geotech. J. 9 (1), 63–80.
Lai, Y., Li, S., Qi, J., Gao, Z., Chang, X., 2008. Strength distributions of warm frozen clay and its stochastic damage constitutive model. Cold Reg. Sci. Technol. 53 (2), 200–215.
Lai, Y., Jin, L., Chang, X., 2009. Yield criterion and elasto-plastic damage constitutive model for frozen sandy soil. Int. J. Plast. 25 (6), 1177–1205.
Lai, Y., Gao, Z., Zhang, S., Chang, X., 2010a. Stress-strain relationships and nonlinear Mohr strength criteria of frozen sandy clay. Soils Found. 50 (1), 45–53.
Lai, Y., Yang, Y., Chang, X., Li, S., 2010b. Strength criterion and elastoplastic constitutive model of frozen silt in generalized plastic mechanics. Int. J. Plast. 26 (10), 1461–1484.
Lai, Y., Xu, X., Dong, Y., Li, S., 2013. Present situation and prospect of mechanical research on frozen soils in China. Cold Reg. Sci. Technol. 87, 6–18.
Lai, Y., Xu, X., Yu, W., Qi, J., 2014. An experimental investigation of the mechanical behavior and a hyperplastic constitutive model of frozen loess. Int. J. Eng. Sci. 84, 29–53.
Lai, Y., Liao, M., Hu, K., 2016. A constitutive model of frozen saline sandy soil based on energy dissipation theory. Int. J. Plast. 78, 84–113.
Lee, M.Y., Fossum, A.F., Costin, L.S., Bronowski, D.R., Jung, J., 2002. Frozen Soil Material Testing and Constitutive Modeling. (No. SAND2002-0524). Sandia National Lab.(SNL-NM), Albuquerque, NM (United States); Sandia National Lab.(SNL-CA), Livermore, CA (United States).
Li, K.Q., He, H.L., 2024. Towards an improved prediction of soil-freezing characteristic curve based on extreme gradient boosting model. Geosci. Front. 15 (6), 101898.

Li, K.Q., Yin, Z.Y., 2024. State of the art of coupled thermo–hydro-mechanical–chemical modeling for frozen soils. Arch. Computat. Meth. Engineering. https://doi.org/10.1007/s11831-024-10164-w.
Li, H., Yang, H., Chang, C., Sun, X., 2001. Experimental investigation on compressive strength of frozen soil versus strain rate. J. Cold Reg. Eng. 15 (2), 125–133.
Li, D.W., Fan, J.H., Wang, R.H., 2011. Research on visco-elastic-plastic creep model of artificially frozen soil under high confining pressures. Cold Reg. Sci. Technol. 65 (2), 219–225.
Li, Y., Song, Y., Yu, F., Liu, W., Wang, R., 2011b. Effect of confining pressure on mechanical behavior of methane hydrate-bearing sediments. Pet. Explor. Dev. 38 (5), 637–640.
Li, Y., Liu, W., Zhu, Y., Chen, Y., Song, Y., Li, Q., 2016. Mechanical behaviors of permafrost-associated methane hydrate-bearing sediments under different mining methods. Appl. Energy 162, 1627–1632.
Li, D., Yang, X., Chen, J., 2017. A study of Triaxial creep test and yield criterion of artificial frozen soil under unloading stress paths. Cold Reg. Sci. Technol. 141, 163–170.
Li, K.Q., Li, D.Q., Li, P.T., Liu, Y., 2019. Meso-mechanical investigations on the overall elastic properties of multi-phase construction materials using finite element method. Constr. Build. Mater. 228, 116727.
Li, K.Q., Li, D.Q., Liu, Y., 2020a. Meso-scale investigations on the effective thermal conductivity of multi-phase materials using the finite element method. Int. J. Heat Mass Transf. 151, 119383.
Li, J., Tang, Y., Feng, W., 2020b. Creep behavior of soft clay subjected to artificial freeze–thaw from multiple-scale perspectives. Acta Geotech. 15 (10), 2849–2864.
Li, D., Zhang, C., Ding, G., et al., 2020c. Fractional derivative-based creep constitutive model of deep artificial frozen soil. Cold Reg. Sci. Technol. 170, 102942.
Li, S.Z., Tang, L., Tian, S., Ling, X.Z., Ye, Y.S., Cai, D.G., 2021a. Mechanical Modeling of Frozen Coarse-Grained Materials Incorporating Microscale Investigation. Adv. Mater. Sci. Eng. 2021, 6639428.
Li, T., Kong, L., Wang, J., Wang, F., 2021b. Trimodal pore structure evolution characteristics and mechanical effects of expansive soil in seasonally frozen areas based on NMR test. Rock Soil Mech. 42, 2741–2754.
Li, B., Zhu, Z., Ning, J., Li, T., Zhou, Z., 2022. Viscoelastic–plastic constitutive model with damage of frozen soil under impact loading and freeze–thaw loading. Int. J. Mech. Sci. 214, 106890.
Li, K.Q., Liu, Y., Yin, Z.Y., 2023a. An improved 3D microstructure reconstruction approach for porous media. Acta Mater. 242, 118472.
Li, K.Q., Yin, Z.Y., Liu, Y., 2023b. Influences of spatial variability of hydrothermal properties on the freezing process in artificial ground freezing technique. Comput. Geotech. 159, 105448.
Li, K., Yin, Z., Zhang, N., Liu, Y., 2023c. A data-driven method to model stress-strain behaviour of frozen soil considering uncertainty. Cold Reg. Sci. Technol. 103906. https://doi.org/10.1016/j.coldregions.2023.103906.
Li, K.Q., Yin, Z.Y., Qi, J.L., Liu, Y., 2024a. State-of-the-art constitutive modeling of frozen soils. Arch. Computat. Meth. Eng. 31, 3801–3842. https://doi.org/10.1007/s11831-024-10102-w.
Li, K.Q., Yin, Z.Y., Jin, Y.F., Liu, Y., 2024b. Investigation on evolution law of frozen wall thickness in artificial ground freezing under seepage conditions. Can. Geotech. J. https://doi.org/10.1139/cgj-2023-0576.
Li, K., Yin, Z., Zhang, N., Liu, H., 2025. Physics-informed neural networks for solving steady-state temperature field in artificial ground freezing. Can. Geotech. J. https://doi.org/10.1139/cgj-2024-0650.
Liao, M., Lai, Y., Liu, E., Wan, X., 2017. A fractional order creep constitutive model of warm frozen silt. Acta Geotech. 12, 377–389.
Ling, X.Z., Zhu, Z.Y., Zhang, F., Chen, S.J., Wang, L.N., Gao, X., Lu, Q.R., 2009. Dynamic elastic modulus for frozen soil from the embankment on Beiluhe Basin along the Qinghai–Tibet Railway. Cold Reg. Sci. Technol. 57 (1), 7–12.
Ling, X., Li, Q., Wang, L., Zhang, F., An, L., Xu, P., 2013. Stiffness and damping radio evolution of frozen clays under long-term low-level repeated cyclic loading: experimental evidence and evolution model. Cold Reg. Sci. Technol. 86, 45–54.
Ling, X.Z., Zhang, F., Li, Q.L., An, L.S., Wang, J.H., 2015. Dynamic shear modulus and damping ratio of frozen compacted sand subjected to freeze–thaw cycle under multi-stage cyclic loading. Soil Dyn. Earthq. Eng. 76, 111–121.
Liu, J.K., Peng, L.Y., 2009. Experimental study on the unconfined compression of a thawing soil. Cold Reg. Sci. Technol. 58 (1–2), 92–96.
Liu, J., Cui, Y., Wang, P., Lv, P., 2014. Design and validation of a new dynamic direct shear apparatus for frozen soil. Cold Reg. Sci. Technol. 106, 207–215.
Liu, X., Liu, E., Zhang, D., Zhang, G., Yin, X., Song, B., 2019. Study on effect of coarse-grained content on the mechanical properties of frozen mixed soils. Cold Reg. Sci. Technol. 158, 237–251.
Liu, X., Qin, H., Lan, H., 2020. On the relationship between soil strength and wave velocities of sandy loess subjected to freeze-thaw cycling. Soil Dyn. Earthq. Eng. 136, 106216.
Liu, Y., Li, K.Q., Li, D.Q., Tang, X.S., Gu, S.X., 2022a. Coupled thermal–hydraulic modeling of artificial ground freezing with uncertainties in pipe inclination and thermal conductivity. Acta Geotech. 17, 257–274.
Liu, X., Wei, X., Qin, H., 2022b. Characterizing compressive strength of compacted saline loess subjected to freeze–thaw cycling with wave velocity. Bull. Eng. Geol. Environ. 81 (4), 168.
Liu, Q., Cai, G., Zhou, C., Yang, R., Li, J., 2024a. Thermo-hydro-mechanical coupled model of unsaturated frozen soil considering frost heave and thaw settlement. Cold Reg. Sci. Technol. 217, 104026.
Liu, F., Ma, W., Zhou, Z., Wen, Z., Mu, Y., Shen, M., He, P., 2024b. Dynamic behaviors of frozen silt under repeated traffic loading. Road Mater. Pavement Des. 25 (5), 1068–1089.
Liu, F., Ma, W., Zhou, Z., Wen, Z., Shen, M., Bai, R., 2025. Experimental investigation of cyclic responses of frozen soil under principal stress rotation induced by wave loads. Cold Reg. Sci. Technol. 230, 104368.
Lyu, C., Grimstad, G., Nishimura, S., 2021a. Pore pressure coefficient in frozen soils. Géotechnique 73 (6), 521–530.
Lyu, C., Nishimura, S., Amiri, S.A.G., Zhu, F., Eiksund, G.R., Grimstad, G., 2021b. Pore-water pressure development in a frozen saline clay under isotropic loading and undrained shearing. Acta Geotech. 16, 3831–3847.
Ma, W., Wu, Z.W., Pu, Y.B., Chang, X.X., 1997. Monitoring the change of structures in frozen soil in triaxial creep process by CT. J. Glaciol. Geocryol. 19 (1), 52–57 (in Chinese).
Ma, W., Wu, Z.W., Pu, Y.B., Chang, X.X., 1998. Monitoring the change of structures in frozen soil during the triaxial creep process by computer tomography. Permafrost-seventh international conference (Proceedings). Canada, Collection Nordicana 55, 697–701.
Ma, W., Wu, Z., Zhang, L., Chang, X., 1999. Analyses of process on the strength decrease in frozen soils under high confining pressures. Cold Reg. Sci. Technol. 29 (1), 1–7.
Ma, D., Ma, Q., Yuan, P., 2017. SHPB tests and dynamic constitutive model of artificial frozen sandy clay under confining pressure and temperature state. Cold Reg. Sci. Technol. 136, 37–43.
Ma, D., Ma, Q., Yao, Z., Huang, K., 2019. Static-dynamic coupling mechanical properties and constitutive model of artificial frozen silty clay under triaxial compression. Cold Reg. Sci. Technol. 167, 102858.
Ma, D., Xiang, H., Ma, Q., Kaunda, E.E., Huang, K., Su, Q., Yao, Z., 2021a. Dynamic damage constitutive model of frozen silty soil with prefabricated crack under uniaxial load. J. Eng. Mech. 147 (6), 04021033.
Ma, Q., Huang, K., Ma, D., 2021b. Energy absorption characteristics and theoretical analysis of frozen clay with pre-existing cracks under uniaxial compressive impact load. Cold Reg. Sci. Technol. 182, 103206.
Miyazaki, K., Yamaguchi, T., Sakamoto, Y., Aoki, K., 2011. Time-dependent behaviors of methane-hydrate bearing sediments in triaxial compression test. Int. J. JCRM 7 (1), 43–48.
Mu, Y., Ma, W., Li, G., Mao, Y., Liu, Y., 2020. Long-term thermal and settlement characteristics of air convection embankments with and without adjacent surface water ponding in permafrost regions. Eng. Geol. 266, 105464.
Nassr, A., Esmaeili-Falak, M., Katebi, H., Javadi, A., 2018. A new approach to modeling the behavior of frozen soils. Eng. Geol. 246, 82–90.
Nguyen, A.D., Sego, C.D., Arenson, U.L., Biggar, W.K., 2010. The dependence of strength and modulus of frozen saline sand on temperature, strain rate and salinity. In: Proceedings of the 63rd Canadian Geotechnical Conference, Calgary, pp. 467–475.
Ning, J., He, Y., Zhu, Z., 2014. Dynamic constitutive modeling of frozen soil under impact loading. Chin. Sci. Bull. 59 (26), 3255–3259.
Nishimura, S., Okajima, S., Wang, J., Joshi, B.R., 2019. Small-strain deformation behavior of a clay at frozen and unfrozen states: A comparative study. In: E3S Web of Conferences, vol. 92. EDP Sciences, p. 04001.
Nishimura, S., Okajima, S., Joshi, B.R., Higo, Y., Tokoro, T., 2021. Volumetric behavior of clays under freeze–thaw cycles in a mesoscopically uniform element. Géotechnique 71 (12), 1150–1164.
Nishimura, S., Kawasaki, H., Sato, I., 2023. On limit strength of frozen clay undergoing triaxial tension. Géotechnique. https://doi.org/10.1680/jgeot.22.00192.
Ogata, N., Yasuda, M., Kataoka, T., 1983. Effects of salt concentration on strength and creep behavior of artificially frozen soils. Cold Reg. Sci. Technol. 8 (2), 139–153.
Orth, W., 1986. Gefrorener sand als werkstoff: Elementversuche und materialmodell, Institut für Bodenmechanik und Felsmechanik Karlsruhe. In: Institut für Bodenmechanik und Felsmechanik der Universität Fridericiana in Karlsruhe: Karlsruhe, Germany, vol. 100.
Parameswaran, V.R., Jones, S.J., 1981. Triaxial testing of frozen sand. J. Glaciol. 27 (95), 147–155.
Park, J.H., Lee, J.S., 2014. Characteristics of elastic waves in sand–silt mixtures due to freezing. Cold Reg. Sci. Technol. 99, 1–11.
Pham, K., Jung, S., Park, S., Kim, D., Choi, H., 2021. Bayesian Neural Network for estimating Stress-Strain Behaviors of Frozen Sand. KSCE J. Civ. Eng. 26 (2), 933–941.
Pharr, G.M., Merwin, J.E., 1985. Effects of brine content on the strength of frozen Ottawa sand. Cold Reg. Sci. Technol. 11 (3), 205–212.
Pitcher, C., Kömle, N., Leibniz, O., Morales-Calderon, O., Gao, Y., Richter, L., 2016. Investigation of the properties of icy lunar polar regolith simulants. Adv. Space Res. 57 (5), 1197–1208.
Qi, J.L., Lai, Y.M., Pu, Y.B., 2003. Experimental study on the micro-fabric of frozen sediment using triaxial deformation and computerized tomography. Ann. Glaciol. 37, 105–107.
Qi, J., Ma, W., 2007. A new criterion for strength of frozen sand under quick triaxial compression considering effect of confining pressure. Acta Geotech. 2, 221–226.
Qiao, H., Zhu, Z., Li, B., 2022. Dynamic constitutive model for unsaturated frozen soil considering the influence of matrix suction. Meccanica 57 (9), 2365–2378.
Qu, H., Mu, D., Ren, Z., Huang, Z., Huang, Y., Tang, A., 2022. Stress–Strain–Time Description and Analysis of Frozen–Thawed Silty Clay under Low Stress Level. Geotechnics 2 (4), 871–907.
Ren, Z., Liu, J., Jiang, H., Wang, E., 2023a. Experimental study and simulation for unfrozen water and compressive strength of frozen soil based on artificial freezing technology. Cold Reg. Sci. Technol. 205, 103711.
Ren, Z., Wang, E., Liu, J., Jiang, H., Yao, Z., 2023b. Characterization and Prediction of Compressive Strength in Ultralow-Temperature Frozen Soil using Nuclear magnetic Resonance and WOA-ENN Model. Transportation Geotechnics 101143.

Ricardo, D., Hodgkinson, J., Rhamdhani, M.A., Brooks, G., 2023. A review on the preparation techniques and geotechnical behavior of icy lunar regolith simulants. Adv. Space Res. https://doi.org/10.1016/j.asr.2023.09.032.

Rist, M.A., Murrell, S.A.F., 1994. Ice triaxial deformation and fracture. J. Glaciol. 40 (135), 305–318.

Romanenko, K.A., Abrosimov, K.N., Kurchatova, A.N., Rogov, V.V., 2017. The experience of applying X-ray computer tomography to the study of microstructure of frozen ground and soils. Earth's Cryosph. 21 (4), 63–68.

Russo, G., Corbo, A., Cavuoto, F., Autuori, S., 2015. Artificial Ground Freezing to excavate a tunnel in sandy soil. Measurements and back analysis. In: Tunnelling and Underground Space Technology incorporating Trenchless Technology Research, 50, pp. 226–238.

Sayles, F.H., 1974. Triaxial Constant Strain Rate Tests and Triaxial Creep Tests on Frozen Ottawa Sand, vol. No. 253. Corps of Engineers, US Army Cold Regions Research and Engineering Laboratory, Hanover, N.H.

Schindler, U., Cudmani, R., Chrisopoulos, S., Schünemann, A., 2023. Multi-stage creep behavior of frozen granular soils: Experimental evidence and constitutive modeling. Can. Geotech. J. https://doi.org/10.1139/cgj-2022-0637.

Shastri, A., Sánchez, M., Gai, X., Lee, M.Y., Dewers, T., 2021. Mechanical behavior of frozen soils: Experimental investigation and numerical modeling. Comput. Geotech. 138, 104361.

Shen, M., Zhou, Z., Zhang, S., 2021. Effect of stress path on mechanical behaviors of frozen subgrade soil. Road Mater. Pavement Des. 23 (5), 1061–1090.

Shen, M., Zhou, Z., Zhang, S., 2022. Effect of stress path on mechanical behaviours of frozen subgrade soil. Road Mater. Pavement Des. 23 (5), 1061–1090.

Shen, M., Zhou, Z., Ma, W., 2023. Experimental and theoretical investigation on the unloading creep behaviors of frozen soil. Rock Mech. Rock. Eng. 56, 5833–5859.

Shi, S., Zhang, F., Feng, D., 2023a. A creep constitutive model for heterogeneous frozen clay foil considering the damage of cryostructure. Fatigue Fract. Eng. Mater. Struct. https://doi.org/10.1111/ffe.14097.

Shi, S., Zhang, F., Feng, D., Lin, C., 2023b. Investigation of mechanical properties and elastoplastic numerical calculation model of frozen soil containing ice lenses. Cold Reg. Sci. Technol. 210, 103843.

Smith, T.R., Schulson, E.M., 1994. Brittle compressive failure of salt-water columnar ice under biaxial loading. J. Glaciol. 40 (135), 265–276.

Sun, Y., Weng, X., Wang, W., Niu, H., Li, H., Zhou, R., 2020. A thermodynamically consistent framework for visco-elasto-plastic creep and anisotropic damage in saturated frozen soils. Contin. Mech. Thermodyn. 33 (1), 53–68.

Sun, Z., Zhang, S., Wang, Y., Bai, R., Li, S., 2022. Mechanical behavior and microstructural evolution of frozen soils under the combination of confining pressure and water content. Eng. Geol. 308, 106819.

Tang, L., Cong, S., Geng, L., Ling, X., Gan, F., 2018. The effect of freeze-thaw cycling on the mechanical properties of expansive soils. Cold Reg. Sci. Technol. 145, 197–207.

Torrance, J.K., Elliot, T., Martin, R., Heck, R.J., 2008. X-ray computed tomography of frozen soil. Cold Reg. Sci. Technol. 53 (1), 75–82.

Vinson, T.S., 1978. Parameter effects on dynamic properties of frozen soils. J. Geotech. Eng. Div. 104 (10), 1289–1306.

Vinson, T.S., Chaichanavong, T., Czajkowski, R.L., 1978. Behavior of frozen clay under cyclic axial loading. J. Geotech. Eng. Div. 104 (7), 779–800.

Vyalov, S.S., Slepak, M.E., Maksimyak, R.V., Chapayev, A.A., 1989. Frozen soil deformations and failure under different loading. In: Proceedings of the Fifth International Symposium on Ground Freezing. Balkema, Rotterdam, pp. 465–471.

Wang, J.C., Wang, Y.J., 1998. A study of the microstructure of frozen soils, Permafrost-seventh international conference (Proceedings), Canada. Collection Nordicana 55, 1115–1118.

Wang, D., Ma, W., Chang, X., 2004. Analyses of behavior of stress–strain of frozen Lanzhou loess subjected to K0 consolidation. Cold Reg. Sci. Technol. 40 (1–2), 19–29.

Wang, D.Y., Ma, W., Chang, X.X., Wang, A.G., 2005. Study on the resistance to deformation of artificially frozen soil in deep alluvium. Cold Reg. Sci. Technol. 42 (3), 194–200.

Wang, J., Nishimura, S., Tokoro, T., 2017. Laboratory study and interpretation of mechanical behavior of frozen clay through state concept. Soils Found. 57 (2), 194–210.

Wang, J., Nishimura, S., Okajima, S., Joshi, B.R., 2019a. Small-strain deformation characteristics of frozen clay from static testing. Géotechnique 69 (9), 816–827.

Wang, P., Liu, E., Song, B., Liu, X., Zhang, G., Zhang, D., 2019b. Binary medium creep constitutive model for frozen soils based on homogenization theory. Cold Reg. Sci. Technol. 162, 35–42.

Wang, J., Zhang, F., Yang, Z.J., 2019c. Anisotropy in small-strain shear modulus of permafrost at rising temperatures. Cold Reg. Sci. Technol. 160, 1–12.

Wang, J., Wang, Q., Lin, S., Han, Y., Cheng, S., Wang, N., 2020a. Relationship between the shear strength and microscopic pore parameters of saline soil with different freeze-thaw cycles and salinities. Symmetry 12 (10), 1709.

Wang, P., Liu, E., Zhi, B., Song, B., 2020b. A macro–micro viscoelastic-plastic constitutive model for saturated frozen soil. Mech. Mater. 147, 103411.

Wang, P., Liu, E., Zhi, B., Song, B., Kang, J., 2022. Creep characteristics and unified macro–meso creep model for saturated frozen soil under constant/variable temperature conditions. Acta Geotech. 17 (11), 5299–5319.

Wang, B., Xu, X., Wang, X., Gu, Q., Chen, T., 2023. Mechanical behavior and strength criterion of frozen silty clay under complex stress paths. Geoderma 435, 116506.

Wang, D., Liu, E., Yang, C., Wang, P., Song, B., 2023a. Micromechanics-based binary-medium constitutive model for frozen soil considering the influence of coarse-grained contents and freeze–thaw cycles. Acta Geotech. https://doi.org/10.1007/s11440-023-01831-6.

Wang, D., Liu, E.L., Yang, C.S., Liu, Y.Q., Zhu, S.X., Yu, Q.H., 2023b. Dynamic mechanical characteristics of frozen subgrade soil subjected to freeze-thaw cycles. J. Mt. Sci. 20 (1), 242–255.

Wardak, M.I., 2021. Mechanical Strength of Pure Ice and Regolith-Ice Composites at Cryogenic Temperature. Doctoral dissertation,. Iowa State University.

Wen, D.Y., Jiang, N.S., Liu, C.K., Lv, Z.Q., 2023. Study of the Influence of Temperature rise on the Microstructure of Frozen Soil based on SEM and MIP. J. Mater. Civ. Eng. 35 (5), 05023001.

Wu, Z.W., Ma, W., 1994. Strength and Creep of Frozen Soils. Lanzhou University Press, Lanzhou (In Chinese).

Wu, Z.W., Ma, W., Pu, Y.B., Chang, X.X., Liao, Q., 1995. CT analysis on structure of frozen soil in creep process. CT Theor. Applicat. 4 (3), 31–34.

Xie, Q., Zhu, Z., Kang, G., 2014. Dynamic stress–strain behavior of frozen soil: experiments and modeling. Cold Reg. Sci. Technol. 106, 153–160.

Xu, G., 2014. Hypoplastic Constitutive Models for Frozen Soil. Ph.D. dissertation,. University of Natural Resources and Life Sciences, Vienna, Austria.

Xu, X., Lai, Y., Liu, F., Chang, X., Dong, Y., 2011a. A study of meahnical test methods of frozen soil. J. Glaciol. Geocryol. 33 (5), 1132–1138 (in Chinese).

Xu, H.Y., Lai, Y.M., Yu, W.B., Xu, X.T., Chang, X.X., 2011b. Experimental research on triaxial strength of polycrystalline ice. J. Glaciol. Geocryol. 33 (05), 1120–1126.

Xu, X., Lai, Y., Zhou, Z., Xie, S., 2014. Laboratory investigation on the deformation and damage characteristics of frozen loess under triaxial cyclic and monotonic loading conditions. J. Glaciol. Geocryol. 36 (5), 1184–1191 (in Chinese).

Xu, X., Dong, Y., Fan, C., 2015. Laboratory investigation on energy dissipation and damage characteristics of frozen loess during deformation process. Cold Reg. Sci. Technol. 109, 1–8.

Xu, G., Wu, W., Qi, J., 2016. An extended hypoplastic constitutive model for frozen sand. Soils Found. 56 (4), 704–711.

Xu, X., Li, Q., Xu, G., 2020b. Investigation on the behavior of frozen silty clay subjected to monotonic and cyclic triaxial loading. Acta Geotech. 15, 1289–1302.

Xu, J., Liu, H., Zhao, X., 2017a. Study on the strength and deformation property of frozen silty sand with NaCl under tri-axial compression condition. Cold Reg. Sci. Technol. 137, 7–16.

Xu, X., Wang, B., Fan, C., Zhang, W., 2020a. Strength and deformation characteristics of silty clay under frozen and unfrozen states. Cold Regions Science and Technology 172, 102982.

Xu, X., Wang, Y., Yin, Z., Zhang, H., 2017b. Effect of temperature and strain rate on mechanical characteristics and constitutive model of frozen Helin loess. Cold Reg. Sci. Technol. 136, 44–51.

Xu, G., Peng, C., Wu, W., Qi, J., 2017c. Combined constitutive model for creep and steady flow rate of frozen soil in an unconfined condition. Can. Geotech. J. 54 (7), 907–914.

Xu, J., Ren, J., Wang, Z., Wang, S., Yuan, J., 2018. Strength behaviors and meso-structural characters of loess after freeze-thaw. Cold Reg. Sci. Technol. 148, 104–120.

Xu, J., Li, Y., Ren, C., Wang, S., Vanapalli, S.K., Chen, G., 2021. Influence of freeze-thaw cycles on microstructure and hydraulic conductivity of saline intact loess. Cold Reg. Sci. Technol. 181, 103183.

Xu, K., Zhang, N., Yin, Z.Y., Li, K., 2025. Finite element-integrated neural network for inverse analysis of elastic and elastoplastic boundary value problems. Computer Methods in Applied Mechanics and Engineering 436, 117695.

Yakushev, V.S., Chuvilin, E.M., 2000. Natural gas and gas hydrate accumulations within permafrost in Russia. Cold Reg. Sci. Technol. 31 (3), 189–197.

Yang, Y., Lai, Y., Chang, X., 2010a. Experimental and theoretical studies on the creep behavior of warm ice-rich frozen sand. Cold Reg. Sci. Technol. 63 (1–2), 61–67.

Yang, Y., Lai, Y., Chang, X., 2010b. Laboratory and theoretical investigations on the deformation and strength behaviors of artificial frozen soil. Cold Reg. Sci. Technol. 64 (1), 39–45.

Yang, Y., Lai, Y., Dong, Y., Li, S., 2010c. The strength criterion and elastoplastic constitutive model of frozen soil under high confining pressures. Cold Reg. Sci. Technol. 60 (2), 154–160.

Yang, Y., Lai, Y., Li, J., 2010d. Laboratory investigation on the strength characteristic of frozen sand considering effect of confining pressure. Cold Reg. Sci. Technol. 60 (3), 245–250.

Yang, Z.J., Still, B., Ge, X., 2015. Mechanical properties of seasonally frozen and permafrost soils at high strain rate. Cold Reg. Sci. Technol. 113, 12–19.

Yang, Y.G., Feng, G., Lai, Y.M., Cheng, H.M., 2016. Experimental and theoretical investigations on the mechanical behavior of frozen silt. Cold Reg. Sci. Technol. 130, 59–65.

Yang, J., Hassanpouryouzband, A., Tohidi, B., Chuvilin, E., Bukhanov, B., Istomin, V., Cheremisin, A., 2019. Gas hydrates in permafrost: Distinctive effect of gas hydrates and ice on the geomechanical properties of simulated hydrate-bearing permafrost sediments. J. Geophys. Res. Solid Earth 124 (3), 2551–2563.

Yang, Z., Zhang, Q., Shi, W., Lu, Z., Tu, Z., Ling, X., 2022. Study of a strength prediction model of unsaturated compacted expansive soil under freeze–thaw cycles. Arab. J. Geosci. 15, 130.

Yao, X., Qi, J., Yu, F., Ma, L., 2013. A versatile triaxial apparatus for frozen soils. Cold Reg. Sci. Technol. 92, 48–54.

Yao, X., Qi, J., Liu, M., Yu, F., 2017. A frozen soil creep model with strength attenuation. Acta Geotech. 12, 1385–1393.

Yao, X., Qi, J., Zhang, J., Yu, F., 2018. A one-dimensional creep model for frozen soils taking temperature as an independent variable. Soils Found. 58 (3), 627–640.

Yao, X., Xu, G., Zhang, M., Yu, F., 2019. A frozen soil rate dependent model with time related parabolic strength envelope. Cold Reg. Sci. Technol. 159, 40–46.

You, Z., Lai, Y., Zhang, M., Liu, E., 2017. Quantitative analysis for the effect of microstructure on the mechanical strength of frozen silty clay with different contents of sodium sulfate. Environ. Earth Sci. 76, 1–11.

Yu, F., Qi, J., Yao, X., Liu, Y., 2013. In-situ monitoring of settlement at different layers under embankments in permafrost regions on the Qinghai–Tibet Plateau. Eng. Geol. 160, 44–53.
Yu, Z., Fang, J., Xu, A., Zhou, W., 2022. The study of influence of freeze-thaw cycles on silty sand in seasonally frozen soil regions. Geofluids 6886108.
Zhang, S., Lai, Y., Sun, Z., Gao, Z., 2007. Volumetric strain and strength behavior of frozen soils under confinement. Cold Reg. Sci. Technol. 47 (3), 263–270.
Zhang, H.D., Zhu, Z.W., Song, S.C., Kang, G.Z., Ning, J.G., 2013. Dynamic behavior of frozen soil under uniaxial strain and stress conditions. Appl. Math. Mech. 34 (2), 229–238.
Zhang, B.L., Wang, D.Y., Zhou, Z.W., Ma, W., Lei, L.L., 2021b. The effect of temperature on dynamic characteristics of frozen clay under principal stress rotation. Advances in Materials Science and Engineering 3127253.
Zhang, N., Xu, K.P., Yin, Z-Y., Jin, Y.F., Li, K.Q., 2025. Finite element-integrated neural network framework for elastic and elastoplastic solids. Computer Methods in Applied Mechanics and Engineering 433, 117474.
Zhang, F., Yang, Z.J., Still, B., Wang, J., Yu, H., Zubeck, H., Aleshire, L., 2018. Elastic properties of saline permafrost during thawing by bender elements and bending disks. Cold Reg. Sci. Technol. 146, 60–71.
Zhang, D., Li, Q., Liu, E., Liu, X., Zhang, G., Song, B., 2019a. Dynamic properties of frozen silty soils with different coarse-grained contents subjected to cyclic triaxial loading. Cold Reg. Sci. Technol. 157, 64–85.
Zhang, G., Liu, E., Chen, S., Song, B., 2019b. Micromechanical analysis of frozen silty clay-sand mixtures with different sand contents by triaxial compression testing combined with real-time CT scanning. Cold Reg. Sci. Technol. 168, 102872.
Zhang, W., Ma, J., Tang, L., 2019c. Experimental study on shear strength characteristics of sulfate saline soil in Ningxia region under long-term freeze-thaw cycles. Cold Reg. Sci. Technol. 160, 48–57.
Yu, X., Zheng, G., Zhou, H., Ma, F., 2024. Analytical solutions for the stability of stone column-supported and geosynthetic-reinforced embankment. Canadian Geotech. J. 62, 1–15.
Zhang, S., Kuang, H., Jin, Z.Y., Xu, G.F., 2020a. An experimental study of the stress-strain characteristics of frozen silty clay with high moisture content. Hydrol. Eng. Geol. 47 (5), 116–124.
Zhang, F., Zhu, Z., Fu, T., Jia, J., 2020b. Damage mechanism and dynamic constitutive model of frozen soil under uniaxial impact loading. Mech. Mater. 140, 103217.
Zhang, F., Zhu, Z., Ma, W., Zhou, Z., Fu, T., 2021. A unified viscoplastic model and strain rate–temperature equivalence of frozen soil under impact loading. J. Mech. Phys. Solids 152, 104413.
Zhang, C., Li, D., Luo, C., Wang, Z., Chen, G., 2022. Research on creep characteristics and the model of artificial frozen soil. Adv. Mater. Sci. Eng. 2891673.
Zhang, F., Zhu, Z., Li, B., 2023a. Soil particle size-dependent constitutive modeling of frozen soil under impact loading. Cold Reg. Sci. Technol. 211, 103879.
Zhang, T., Zhu, Z., Li, B., Zhang, F., Li, T., 2023b. A dynamic constitutive model of unsaturated frozen soil with coupled frictional sliding and damage evolution of local cracks. Cold Reg. Sci. Technol. 213, 103907.
Zhang, Y.Z., Liu, W.L., Wang, J.Z., Wang, M., Zhu, D.P., Dong, Y.Q., 2023c. Experimental study on frost heave characteristics and micro-mechanism of fine-grained soil in seasonally frozen regions. Cold Reg. Sci. Technol. 103990.
Zhao, X., Zhou, G., 2013. Experimental study on the creep behavior of frozen clay with thermal gradient. Cold Reg. Sci. Technol. 86, 127–132.
Zhao, X., Zhou, G., Lv, Z., 2019. Radial thermal gradient–dependent deformation behaviors of frozen hollow cylinder. J. Cold Reg. Eng. 33 (1), 04018015.
Zhao, Y., Lai, Y., Pei, W., Yu, F., 2020. An anisotropic bounding surface elastoplastic constitutive model for frozen sulfate saline silty clay under cyclic loading. Int. J. Plast. 129, 102668.
Zhao, L., Peng, J., Ma, P., Leng, Y., Ma, Z., 2023. Microstructure response to shear strength deterioration in loess after freeze-thaw cycles. Eng. Geol. 323, 107229.
Zhou, Z., Ma, W., Zhang, S., Du, H., Mu, Y., Li, G., 2016. Multiaxial creep of frozen loess. Mech. Mater. 95, 172–191.
Zhou, Z., Ma, W., Zhang, S., Mu, Y., Li, G., 2018. Effect of freeze-thaw cycles in mechanical behaviors of frozen loess. Cold Reg. Sci. Technol. 146, 9–18.
Zhou, Z., Ma, W., Zhang, S., Mu, Y., Li, G., 2020. Experimental investigation of the path-dependent strength and deformation behaviours of frozen loess. Eng. Geol. 265, 105449.
Zhou, Z., Zhao, J., Tan, Z., Zhou, X., 2021. Mechanical responses in the construction process of super-large cross-section tunnel: a case study of Gongbei tunnel. Tunn. Undergr. Space Technol. 115, 104044.
Zhu, Y., Carbee, D.L., 1984. Uniaxial compressive strength of frozen silt under constant deformation rates. Cold Reg. Sci. Technol. 9 (1), 3–15.
Zhu, Z., Kang, G., Ma, Y., Xie, Q., Zhang, D., Ning, J., 2016. Temperature damage and constitutive model of frozen soil under dynamic loading. Mech. Mater. 102, 108–116.
Zhu, Z., Liu, Z., Xie, Q., Lu, Y., Li, D., 2017. Dynamic mechanical experiments and microstructure constitutive model of frozen soil with different particle sizes. Int. J. Damage Mechan. 27 (5), 686–706.
Zhu, Z.Y., Luo, F., Zhang, Y.Z., Zhang, D.J., He, J.L., 2019a. A creep model for frozen sand of Qinghai-Tibet based on Nishihara model. Cold Reg. Sci. Technol. 167, 102843.
Zhu, Z., Cao, C., Fu, T., 2019b. SHPB test analysis and a constitutive model for frozen soil under multiaxial loading. Int. J. Damage Mechan. 29 (4), 626–645.
Zhu, Z., Jia, J., Zhang, F., 2020. A damage and elastic-viscoplastic constitutive model of frozen soil under uniaxial impact loading and its numerical implementation. Cold Reg. Sci. Technol. 175, 103081.
Zhu, Z., Fu, T., Zhou, Z., Cao, C., 2021a. Research on Ottosen constitutive model of frozen soil under impact load. Int. J. Rock Mech. Min. Sci. 137.
Zhu, Z.W., Tang, W.R., Kang, G.Z., 2021b. Dynamic deformation of frozen soil at a high strain rate: experiments and damage-coupled constitutive model. Acta Mechanica Solida Sinica 34 (6), 895–910.